Periodico di Mineralogia (2013), 82, 2, 263-290 DOI: 10.2451/2013PM0016

PERIODICO di MINERALOGIA
established in 1930

An International Journal of
MINERALOGY, CRYSTALLOGRAPHY, GEOCHEMISTRY, ORE DEPOSITS, PETROLOGY, VOLCANOLOGY
and applied topics on *Environment*, *Archaeometry* and *Cultural Heritage*

Petrology and geochemistry of the Mamakan gabbroic intrusions, Urumieh (Urmia), Iran: Magmatic development of an intra-oceanic arc

Abdolnaser Fazlnia* and Abouzar Alizade

Department of Geology, University of Urmia, 57153-165 Urmia, Islamic Republic of Iran
*Corresponding author: *a.fazlnia@urmia.ac.ir* and *nfazlnia@yahoo.com*

Abstract

The Mamakan gabbroic intrusions in the northwest of Iran were intruded into Paleozoic platform rocks at 303-298 Ma in the northern part of the Sanandaj-Sirjan shear zone (SSSZ) of central Iran. These intrusions are divided into the layered and massive gabbros. Layered gabbros are interspersed with lenticular bodies of anorthosite and hornblendites that have either gradational or sharp boundaries with the gabbros. There is no obvious deformation in the Mamakan gabbroic intrusions. Hence, the changes in mineral compositions are interpreted as the result of crystallization processes, such as fractionation in the magma chamber. The Mamakan intrusions are a bimodal Hercynian appinitic suite. Hornblende-bearing pegmatitic gabbros, hornblende-bearing gabbros (massive and layered types), ultramafic rocks such as wehrlite, hornblendites, and hornblende peridotites are coeval with peraluminous granitoid rocks in the study area. The abundance of hornblende relative to plagioclase, olivine and pyroxene in rocks of mafic composition, the widespread development of mafic pegmatites (hornblendites) and hornblende-bearing massive and layered gabbros are taken to indicate that the Mamakan appinitic mafic magmas are unusually enriched in H_2O. Geochemical data show that the intrusions were formed from an Al-, Sr-, Mg-, Fe-enriched and K-, Nb-, Ta-, and P- depleted tholeiitic basaltic magma. The rocks show marked negative High Field Strength Elements (HFSE: P, Zr, Hf, Nb, and Ta) and positive Ba and K anomalies that are typical of subduction-related magmas. The magma resulted from the partial melting of a metasomatized spinel peridotite wedge as a result of the beginning of Paleotethys subduction beneath the Mamakan island arc. This island arc was developed over supra-subduction oceanic crust between Gondwanaland and the Paleozoic platform of central Iran (south part of Eurasia).

Key words: Layered gabbro; massive gabbro; hornblendite; fractional crystallization; subduction zone; island arc.

Introduction

Recent studies on continental crustal growth processes and oceanic island-arc formation have revealed that, during the past ~500 million years, accretion of island arcs to existing continents is one of the main geological processes that can contribute to continental crustal growth (e.g., Suyehiro et al., 1996; Sigmarsson et al., 1998; Schaltegger et al., 2002; Dhuime et al., 2009; Petterson, 2010; Guarino et al., 2011). Island arc magmatism that generated above a subducting oceanic plate may be derived either from the slab or from the overlying mantle wedge or both. Evidence from active subduction systems suggest that slab melting is a rare process restricted to hot and young slabs (Sigmarsson et al., 1998; Schaltegger et al., 2002; Dhuime et al., 2009; Petterson, 2010; Guarino et al., 2011). Melts are commonly formed in the overlying mantle wedge, triggered by fluid release from the subducted slab. The mantle source of primary arc melts is considerably more depleted than typical mid-ocean ridge basalt (MORB)-type reservoirs (e.g. Davidson, 1996; Nicotra et al., 2011; Romengo et al., 2012) and therefore requires unrealistically high temperatures to melt further (Schaltegger et al., 2002). Arc magmatism lasting over millions of years implies either rehydration and (re)fertilization of previously depleted mantle or the tapping of new fertile reservoirs developed the evolution of the arc (Schaltegger et al., 2002; Dhuime et al., 2009). Therefore, insights into arc magmatism rely principally on the geochemical trends of volcanic rocks, seismic imaging of active arcs, and the exposure of accreted arc plutonic rocks to understand active processes at depth.

As a result of the growth and development of the island arc, participation of more than one source magma, local dehydration melting metamorphic reactions, magmatic underplating, variation of partial melting in the mantle wedge and changes in magma source occur (Peate et al., 1997; Bignold et al., 2006; Nicotra et al., 2011; Guarino et al., 2011; Romengo et al., 2012). Many of the evolved magmatic compositions of an intra-oceanic arc are a result of fractional crystallization processes of a basic magma (Guarino et al., 2011; Romengo et al., 2012). Gabbros commonly produce successive processes occurring during building of a complete oceanic-island arc system.

Gabbroic cumulate xenoliths that are banded with adcumulate textures have been reported from many tholeiitic and calc-alkaline volcanic rocks from oceanic or continental island arc settings, including the Lesser Antilles (e.g., Arculus and Wills, 1980), the Aleutians (e.g., Conrad and Kay, 1984; Bacon et al., 2007), the Talkeetna Arc (e.g., Burns, 1985; Hacker et al., 2008; Rioux et al., 2010), the Kohistan arc in Northern Pakistan (e.g. Bard et al., 1980; Treloar et al., 1996), and Arenal volcano in Costa Rica (Beard and Borgia, 1989). They indicate that layered gabbro plutons form at depth beneath island arc volcanoes, just as they do in other areas of basaltic volcanism (Gill, 2010).

Southern Iran can be divided into a set of three parallel NW-SE trending tectonic zones (Alavi, 1994; Mouthereau et al., 2012), namely, the Zagros Fold-Thrust belt (ZFTB), the Sanandaj-Sirjan shear zone (SSSZ), and the Tertiary-Quaternary Urumieh-Dokhtar magmatic arc (UDMA; Figure 1). The Zagros is the largest mountain belt and the most active collisional orogen associated with Arabia/Eurasia convergence. It belongs to the Alpine-Himalayan orogenic system that resulted from the closure of the Neotethys Ocean during the Cenozoic (Mouthereau et al., 2012). The tectonic history of these zones as a part of the Tethyan region has been summarized by many authors (e.g., Berberian and King, 1981; Alavi, 1994; Omrani et al., 2008; Khadivi et al., 2012; Mouthereau et al., 2012). The Mamakan gabbroic intrusions are located in the boundary between the north SSSZ-north UDMZ of Iran (Figure 1). The UDMZ is

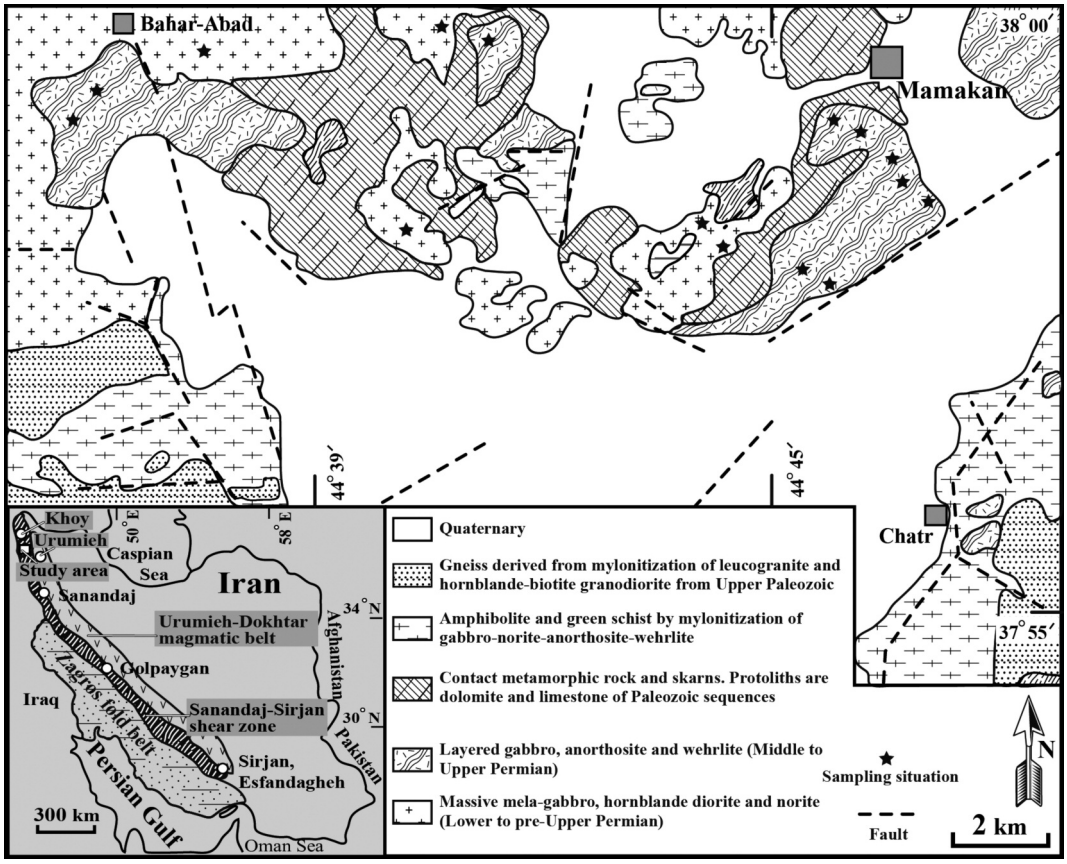

Figure 1. Simplified geological map of northwestern Urumieh (modified after Ghaemi, 2004). Inset shows main tectonic units of Iran.

approximately similar to the SSSZ in length and width. The SSSZ extends over 1500 km, with an average width of 200 km, from Urumieh in the northwest of Iran to Sirjan in the southeast (Figure 1). The SSZ is bordered by the Zagros fold belt to the west and the western central Iran belt (UDMZ) to the east (Berberian and King, 1981; Alavi, 1994; Mohajjel et al., 2003).

The purpose of this paper is to describe the fundamental structural, textural, petrographic, and geochemical aspects of the Mamakan crustal gabbroic intrusions cropped out between the north SSSZ-north UDMZ of Iran (Figure 1).

Geological setting

The Zagros collision zone is located at the tectonic crossroads of the Alpine-Himalayan belts. Its formation results from the large-scale convergence between Eurasia and Gondwanan - derived fragments, as exemplified by accreted ophiolitic belts. As for other segments of the Alpine-Himalayan belts, the Zagros collision zone formed as a result of the disappearance of the Neo-Tethys Ocean (e.g., Alavi, 1994; Berberian and King, 1981; Dercourt et al., 1993; Stampfli and Borel, 2002; Mohajjel et al., 2003;

Agard et al., 2005; Monsef et al., 2010; Agard et al., 2011; Mouthereau et al., 2012) between Arabia and Eurasia. There is a growing body of evidence in support of Late Eocene to Oligocene initial collision (e.g., Agard et al., 2005; Ballato et al., 2010; Agard et al., 2011; Mouthereau et al., 2012). The position of the suture zone between Arabia and Eurasia, regarded by most authors to lie along the Zagros Thrust (Figure 1; Stöcklin, 1968; Agard et al., 2005; Paul et al., 2010), is also still discussed (Alavi, 1994). Three major tectonic elements - the Zagros Fold-Thrust Belt, the Sanandaj-Sirjan shear zone, and the Urumieh-Dokhtar magmatic arc (Alavi, 1994; Figure 1) - are recognized in northwestern, western, and southwestern Iran as being related to the subduction of Neo-Tethyan oceanic crust and subsequent collision of the Arabian plate with the central Iran microplate.

The SSSZ is a narrow zone of highly deformed rocks located between the towns of Sirjan and Esfandagheh in the southeast and Urumieh and Sanandaj in the northwest (Mohajjel et al., 2003). The rocks in this zone are the most highly deformed of the Zagros belt, and share the NW-SE trend of surrounding structures. The zone is dominated by Mesozoic rocks; Palaeozoic rocks are generally rare, but are common in the southeast (Berberian, 1995). The SSSZ is characterized by metamorphosed and complexly deformed rocks associated with abundant deformed and undeformed plutons, as well as widespread Mesozoic volcanic rocks.

The Tertiary Urumieh-Dokhtar magmatic zone (UDMZ) trends NW-SE, parallel to the Zagros Thrust belt in the west of Iran between the SSSZ and the central Iran zone. This narrow zone of arc volcanoplutonic rocks is located in the west border of the central Iran zone (e.g., Berberian and King, 1981; Mohajjel et al., 2003). Magmatism in the UDMA occurred mainly during the Eocene but later resumed, after a dormant period, during the Upper Miocene to Plio-Quaternary. The UDMZ, which records almost continuous calc-alkaline magmatic activity from Eocene to present (e.g., Berberian and King, 1981) peaked during the Oligo-Miocene.

The Mamakan gabbroic intrusions (Figure 1), located northwest of Urumieh, are part of the northern SSSZ (Stöcklin, 1968). Based on Alavi-Naeini (1972), the area is located between the central Iran zone in the east and the SSSZ in the west. According to the Nabavi (1976) the area is located in the Khoy-Mahabad zone (northern part of the SSSZ). Lithologically, the area shows characteristics, such as rock types, outcrops, and structures, of three zones in central Iran, Sanandaj-Sirjan, and Alborz in Azerbaijani province (Ghaemi, 2004). Many previous authors, who have commented about this area, have built their thoughts based on the researches of Haghipour and Aghanabati (1976) and 1:250000 quadrangle map of Seru (Haghipour and Aghanabati, 1976). Based on these researchers, many metamorphic rocks in this area were formed in the Precambrian. On the other hand, formation of the rocks has been related to the Paleozoic events based on Ghaemi (2004). He showed that the granitic-gabbroic intrusions were injected to the metamorphic rocks at the upper Paleozoic. Therefore, based on Ghaemi (2004), the study area was probably the edge of the Paleozoic platform of central Iran. This part of the central Iran is known as the UDMZ. The main characteristics of Sanandaj-Sirjan shear zone cannot be seen in the study area, but can be said that this area is the northwestern boundary of Sanandaj-Sirjan shear zone (Ghaemi, 2004).

The Paleozoic platform of the central Iran was affected by tensile forces resulted from ascending the mantle diapirs in the Upper Paleozoic (Ghaemi, 2004). As a result of this process, continental rifting was developed into the area and crustal thinning occurred as well as basaltic magmas were formed from the upper mantle. Additionally, there are peraluminous

granites synchronous with the mafic magmatism in the area. They are in contact or intercalated with gabbroic rocks (Ghaemi, 2004; Asadpour, 2012; also see below).

Based on field observations (Ghaemi, 2004), the Mamakan gabbros can be subdivided into: a) layered gabbro, which includes ultramafic rocks, and b) massive gabbro (Figure 2A). They show different outcrops in the field. The Mamakan layered gabbros (Figure 2B) along with massive gabbros and minor ultramafic rocks are all products of an injection of mafic magma (co-magmatic process) and evolved in a Paleozoic magma chamber (Ghaemi, 2004). Mafic and ultramafic rocks of the Mamakan intrusions are composed of gabbro, anorthosite, wehrlite, hornblendite, and hornblende diorite (Figures 1 and 2). According to Ghaemi (2004), wehrlite, dunite and harzburgite were altered to the hornblende- or serpentine-rich rocks during metasomatism. Therefore, many of the rocks are now hornblendite (Figure 2F). Amphibole in hornblendite is edenitic in composition (Ghaemi, 2004).

Intrusion of the gabbroic magmas into mature crust increased heat flow, causing partial melting at the base of the crust and the generation of granitic magmas. Thus bimodal magmatism was synchronous with crustal extension (Ghaemi, 2004). After these events, movement along shear zones caused widespread mylonitization in all rock types of the central Iranian platform (Ghaemi, 2004).

Magma mixing and magma mingling have occurred between the gabbroic (massive gabbros) and granitic liquids in the study area (Figure 2A). Asadpour (2012, in press) determined U-Pb zircon Laser-Ablation ages of the massive gabbros as *c.* 300.7±1.5 Ma and leuco-granites as *c.*300.3±1.5 Ma. Therefore, all rock types (gabbros and granitoids) were formed in the Late Carboniferous. Layered gabbros are slightly older (301.5±1.3 Ma) than massive gabbros (Asadpour, 2012, in press). Therefore, it is likely that these intrusions have the same source and display bimodal distribution of magma types (Ghaemi, 2004; also see Figure 2A). On the other hand, based on Asadpour (2002) and Ghaemi (2004), the influence of the mafic magma on the continental crust in the central Iran caused to the base of the crust undergo partial melting to create granitic magma.

According to Khalatbari-Jafari et al. (2006), there are two ophiolitic complexes in the Khoy area (60-70 km north of the study area is): (1) an older poly-metamorphic ophiolite, tectonically included within a metamorphic subduction complex, whose oldest metamorphic amphiboles yield a Lower Jurassic (*c.* 194.8±10.1 Ma) ^{40}K-^{40}Ar as an apparent age. Accordingly, primary magmatic age should logically be pre-Jurassic (Late Permian-Triassic?), and provide a minimum age for the intrusion; (2) a younger and non metamorphic ophiolite of Upper Cretaceous age (102.1±5.4 Ma based on magmatic amphiboles), overlain by a turbiditic, flysch-like volcanogenic series, of Late Cretaceous-Early Paleocene age.

Field observations

The Mamakan layered gabbroic-ultramafic complex has several rock types in the field. The complex is mainly composed of alternating layers of gabbro, gabbro-norite, minor wehrlite, and anorthosite. Boundaries between the rocks of the complex may be sharp or gradational. Minerals in the rocks are crystallized in laminae (tabular or platy). Layered mafic and ultramafic intrusions often contain layer-parallel fabrics defined by the planar arrangements of tabular or platy cumulus minerals (mineral lamination). Based on the abundances of mafic minerals, the gabbros are separable into leuco-, meso- and mela-gabbro (Figures 2B, 2C). In most outcrops, the boundaries between gabbro types are gradational and the rock composition changes from mela- to leuco-gabbro (Figure 2C). In some

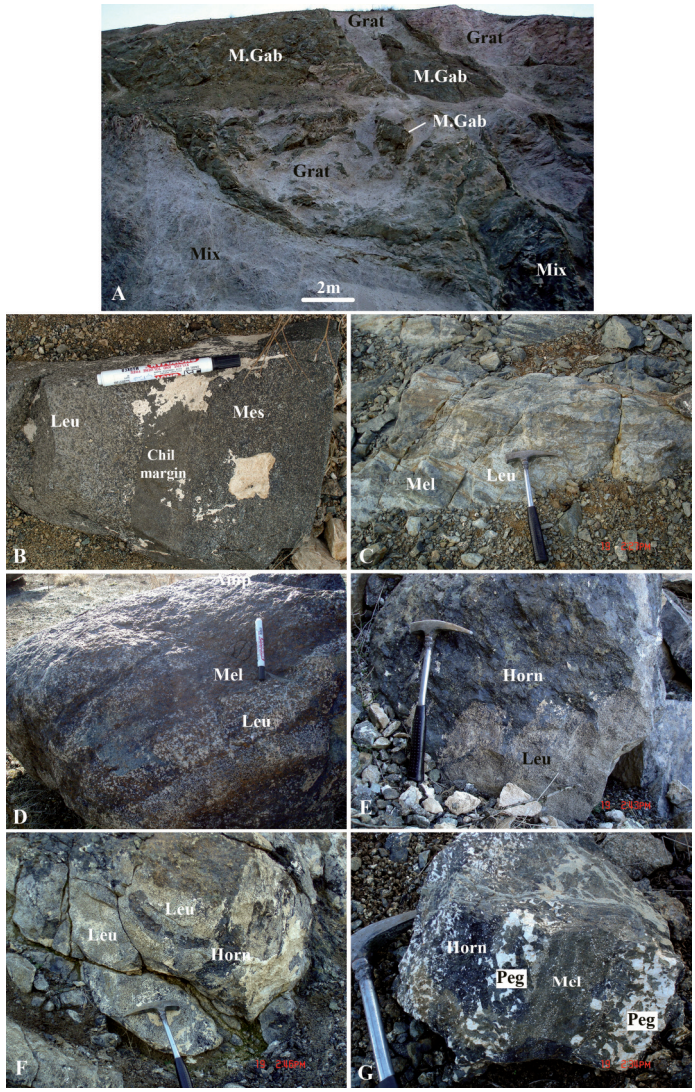

Figure 2. Photographs from some rock types. A) Outcrop showing magma mixing between massive gabbro and leuco-granite. This photo shows that these rocks formed simultaneously; B, C, and D) Bands with different mineral proportions, probably as a result of gravitational settling, new melt percolation, and convection. In B chilled margin of meso-gabbro injected in leuco-gabbro is visible. Therefore, meso-gabbro was s a new melt that cross cut leuco-gabbro. There is in D a segregation via infiltration feature; E) Outcrop of hornblendite within layered gabbros with a sharp boundary; F) Lenticular outcrops of hornblendite within leuco-gabbro from layered rock types. Figures D and F show that the hornblendites do not formed as a result of metasomatism process within the shear zones; G) Alternation of mela-gabbro, pegmatite gabbro, and hornblendite outcrops. This figure shows rapid and irregular variations in texture on a hand-specimen scale from mafic pegmatite to fine grained gabbro. Abbreviations: Mix = magma mixing, Grat = leuco-granite, M.Gab = massive gabbro, Leu = leuco-gabbro, Mes = meso-gabbro, Mel = mela-gabbro, Horn = hornblendite, Peg = pegmatite, Chil margin = chilled margin.

gabbro outcrops, mela-gabbro has lenticular shapes within leuco-gabbro (Figure 2C). Sharp and gradational borders with other types of gabbro are visible (Figure 2D).

No sign of metamorphism was observed in the Mamakan gabbroic intrusions but a strong, mylonitic deformation is however visible in some gabbroic outcrops. Some of the rocks from numerous outcrops are extremely mylonitic and/or have changed to amphibolite and green schist only in texture.

Petrographic observations

Based on the field observations, the Mamakan gabbroic intrusions are divided into the layered and massive types. The Mamakan massive gabbroic intrusions show magma mixing (Figure 2A) or sharp boundaries with leuco-granitoids (Figure 3A). There are gradational (Figure 2A, right and center lower parts) and sharp (Figure 2A, upper part) boundaries in the location of the magma mixing and magma mingling, respectively. Hybrid samples show a mineral assemblage from each of the two end members, with variation in plagioclase, K-feldspar, clinopyroxene, biotite, hornblende, and quartz. Massive gabbros are composed of clinopyroxene, plagioclase, and hornblende along with accessory minerals of titanite and opaques, and granular texture (Figure 3B).

Occurrence of biotite-amphibole-bearing rims around granitic lenses mingled or mixed with massive gabbros rocks (Figure 3A) exhibit metasomatic exchanges in the boundaries between granitic and mafic magmas.. Rims of biotite-calcite around granitic lenses formed by movement of Fe, Mg, Ca, Mn, and CO_2-bearing fluid from mafic magma and of Na, K, Si, and Al from granitic magma toward the boundaries. These rims are present only around granitic lenses. Therefore, exchang of ions between the rocks at the boundaries of mingling and mixing are main cause of formation of the rims. Mingling and mixing between layered gabbros and granites were not found in this research.

Mineral assemblages in the layered and massive gabbros consist mainly of plagioclase (15-60 vol.%), clinopyroxene (15-50 vol.%), and olivine (5-35 vol.%) (Figure 4A, B). Hornblende (2-20 vol.%) and minor amounts of biotite (less than 1 vol.%) are present in some of the layered gabbros and some of the other rock types, such as hornblendite and massive gabbros (Figure 4C, D). In most samples, orthopyroxene is either absent or present with a small amount. The layered

Figure 3. A) Occurrence of biotite-amphibole-bearing rims around leuco-granitic lenses; B) Massive gabbro from the Mamakan complex.

gabbros are coarse-grained and the main minerals are mostly euhedral (Figure 4D). The main textures in the gabbros are granular and cumulate (Figures 4A-D) but an ophitic texture is also present in some places (also see the texture in Figure 4E from hornblendite). Where contact boundaries among different gabbros are gradational, modal percentages of plagioclase, olivine, and clinopyroxene change gradually. Where these contact boundaries are sharp, these changes are sharp. Also, hornblendites are cumulate and exhibit ophitic textures. Also, they are dominated by hornblende. Hornblendites (Figure 2E, G) are characterized by large hornblende crystals that poikilitically enclose plagioclase (2-4 vol.%), olivine (2-3 vol.%), and clinopyroxene (4-5 vol.%; Figure 4E). Some of the hornblendites have small swarms of hornblende-bearing pegmatitic gabbroic lenses with either gradational or sharp boundaries (Figure 2G). Hornblende pegmatites are dominated by black idiomorphic hornblende and white plagioclase with minor clinopyroxene. They occur only along with hornblendites (Figure 2G). These characteristics suggest presence of H_2O and fractional crystallization in these rocks during formation (see appinite suits investigated by Murphy, 2013).

Anorthosites are composed mainly of plagioclase (Figure 4F) along with small percentages of olivine and clinopyroxene. Where the boundaries between these rocks and gabbro are gradational, changes in modal percentages of plagioclase, olivine, and clinopyroxene are marked. At the gradational boundaries between anorthosites and gabbros, gabbros gradually change from meso-gabbro, leuco-gabbro, olivine-clinopyroxene-bearing anorthosite and finally into anorthosite. At boundaries where the rock composition changes abruptly, the modal percentages of the original minerals also decrease or increase abruptly (Figures 2B-F). These rocks are coarse-grained and their main textures are granular and cumulate (Figure 4F). In some places, small hornblende-rich lenses are present in these rocks and in the leuco-gabbros (Figure 2E). The anorthosites are clearly related to the gabbros and occurred only along layered gabbros. The boundaries between these rocks and gabbros are gradational. Reaction corona between olivine and plagioclase are a common feature of many Mamakan layered gabbroic rocks (Figures 4A, B). The corona consists only of an orthopyroxene rim.

Massive gabbros are all mela-gabbro in composition. They have no gradational boundaries with layered gabbros. The boundaries are sharp as parallel planes without mingling between them. Mineralogically, they are similar to the gabbroic parts of the layered gabbros, but they have a higher percentage of hornblende and no layering is visible. More clinopyroxenes in the massive gabbros underwent low temperature re-equilibration or metasomatic process to be changed into the amphibole.

Rock geochemistry

Analytical methods

The rock samples were powdered in an agate mill. LOI (Loss Of Ignition) was determined by heating powders at 1000 °C for 2 hours. The decreased weights of the powders were then calculated. Table 1 lists the chemical compositions of 15 representative samples obtained by ICP-MS (inductively coupled plasma-mass spectrometry). The major and trace elements of samples were analysed with an ICP-MS instrument at the ALS Chemex Company of Canada (website: www.alsglobal.com; Certificate: SV12055502).

Layered gabbros

The Mamakan mela-, meso-, and leuco-gabbros show wide ranges in MgO, Fe_2O_3*, CaO, and Al_2O_3 content (Table 1; Figures 5A-D). Contents of MgO (Figure 5A), Fe_2O_3* (Figure 5D), and Na_2O (Figure 5E) in the layered

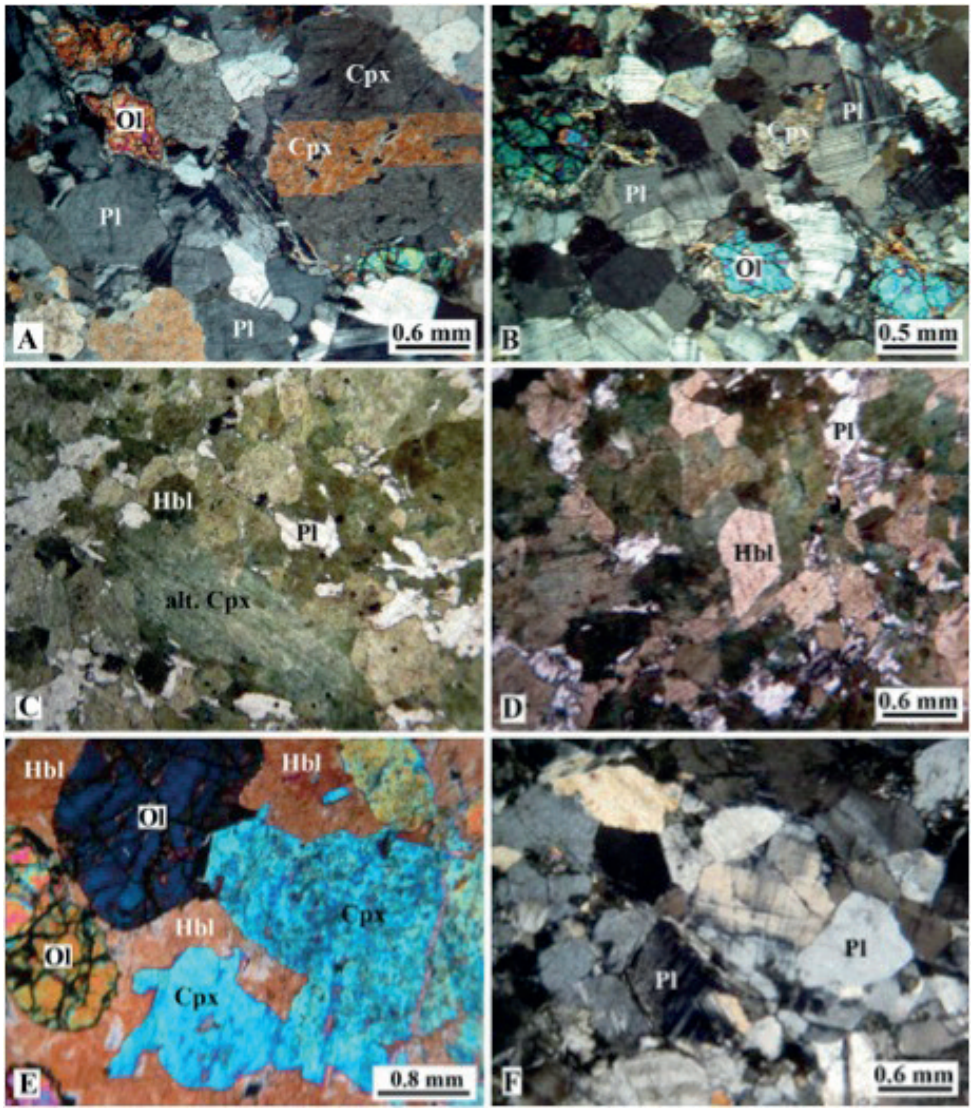

Figure 4. Photographs from the Mamakan gabbroic intrusions. A and B) Mineral assemblages in the layered and massive gabbros, respectively, consist mainly of plagioclase, clinopyroxene, and olivine (XPL light). There are reaction corona between olivine and plagioclase. The corona consists only of an orthopyroxene rim; C and D) Occurrence of altered clinopyroxene (as uralitization), hornblende, and plagioclase in the hornblendite (in layered gabbros) and massive gabbros (PPL light); E) Ophitic texture in layered gabbros (PPL light); F) Mineral assemblages in the anorthosite (XPL light). Mineral abbreviations are: Cpx = clinopyroxene; Hbl = hornblende; Ol = olivine; alt.Cpx = altered clinopyroxene; Pl = plagioclase.

Table 1. Representative whole rock geochemical analyses (ICP-MS) of major elements from the Mamakan rocks.

Sample		FM-2	FM-5	FM-6	FM-9	FM-11	FM-12	FM-15	FM-22	FM-25	FM-26	FM-30	FM-31	FM-32	FM-35	FM-36
	Uncertainty	Meso	Mela	Hornb	Leuco	Leuco	Leuco	Leuco	Hornb	Hornb	Cpx-Ano	Mela	Mela	Mela	Mela	Mela
Rock type	%	Lay-G	Lay-G	Lay-G	Lay-G	Lay-G	Lay-G	Lay-G	Lay-G	Lay-G	Lay-G	Mas-G	Mas-G	Mas-G	Mas-G	Mas-G
SiO_2	0.01	43.10	43.70	44.90	44.20	44.70	44.80	45.30	46.10	47.90	44.60	47.30	46.30	45.30	47.20	47.60
TiO_2	0.01	0.17	0.17	1.13	0.10	0.15	0.12	0.13	0.45	0.37	0.07	0.93	1.14	0.98	0.78	0.87
Al_2O_3	0.01	21.80	18.40	7.36	28.50	23.30	26.70	26.10	8.38	3.97	29.50	12.80	13.15	13.20	11.15	13.10
MgO	0.01	8.48	13.10	18.35	4.23	7.53	4.33	5.39	18.05	20.70	2.73	10.35	9.44	10.45	12.60	9.45
Fe_2O_3*	0.04	4.91	7.59	10.90	2.91	4.58	3.02	3.10	9.81	11.35	2.00	11.45	13.10	11.60	11.95	10.75
MnO	0.01	0.08	0.12	0.16	0.05	0.07	0.05	0.05	0.16	0.20	0.03	0.18	0.21	0.19	0.20	0.19
CaO	0.01	16.85	15.50	15.05	17.50	16.95	17.95	17.90	14.45	14.55	18.25	14.30	12.60	12.75	12.50	14.25
Na_2O	0.01	0.58	0.50	0.95	0.69	0.59	0.90	0.64	0.55	0.38	0.77	1.67	1.79	1.48	1.65	1.56
K_2O	0.01	0.05	0.14	0.19	0.02	0.05	0.13	0.04	0.09	0.07	0.06	0.57	0.54	0.54	0.39	0.61
P_2O_5	0.01	0.01	0.01	0.01	0.02	0.01	0.01	0.01	0.01	0.02	0.01	0.14	0.21	0.13	0.15	0.14
Total	0.01	96.03	99.23	99.00	98.21	97.93	98.01	98.66	98.05	99.51	98.02	99.69	98.48	96.62	98.57	98.52
LOI		2.46	2.44	1.07	1.01	2.00	1.82	1.05	2.40	0.94	1.45	1.20	1.40	1.83	1.55	1.29
FeO*		4.42	6.83	9.81	2.62	4.12	2.72	2.79	8.83	10.21	1.80	10.30	11.79	10.44	10.75	9.67
FeO*/MgO		0.52	0.52	0.53	0.62	0.55	0.63	0.52	0.49	0.49	0.66	1.00	1.25	1.00	0.85	1.02
X_{Mg}		0.66	0.66	0.65	0.62	0.65	0.61	0.66	0.67	0.67	0.60	0.50	0.44	0.50	0.54	0.49

Note: Fe_2O_3* = Fe_2O_3 total; FeO* = FeO total; X_{Mg} = MgO/(MgO+FeO*); LOI = Loss Of Ignition; Meso = Meso-gabbro; Mela = Mela-gabbro; Hornb = Hornblendite; Leuco = Leuco-gabbro; Lay-G = Layered gabbro; Mas-G= Massive gabbro; Cpx-Ano = Cliopyroxene anorthosite.

gabbros are lower than in the massive gabbros and hornblendites. Both rock types have lower contents of K_2O in comparison with massive gabbros. There are increasing contents of SiO_2, Al_2O_3, CaO, Na_2O, and K_2O and decreasing contents of FeO*, MgO, and MnO from gabbros towards anorthosites. Clinopyroxene-bearing anorthosite (FM-26) is geochemically similar to the other gabbros.

High normative hypersthene (C.I.P.W. norm) in some of the gabbros and other rock types (Table 3) indicate that they are related to the tholeiitic suite (Figure 6A, B).

Concentrations of Sr in the leuco-gabbros are higher than those of meso- and mela-gabbros. On the other hand, concentrations of Co, Cr, and Ni (Figures 5H-G) in the leuco-gabbros are lower than those of meso- and mela-gabbros. High concentrations of Sr and Ba (Figures 5H-G) are related to high contents of Na_2O, Al_2O_3, and CaO.

The gabbros show positive Sr and Ba and negative Nb and P anomalies (Figure 7A). The gabbroic rocks are not strongly enriched in LREEs (light REE; Figure 8A).Therefore, there are low La_n/Yb_n ratios (Table 2) and flat HREE patterns in the gabbros (Figure 8A).There are the high Eu/Eu* ratios of the leuco-gabbros (average 2.30) in relation to the meso-gabbros (1.79) and mela-gabbros (1.53). The gabbros show negative Nb, Zr, and P anomalies.

Hornblendite in layered gabbros

Hornblendite in layered gabbros can be distinguished from other rock types based on their major element abundances (Figure 5). Contents of MgO, Al_2O_3, and K_2O in hornblendites are plotted in different positions. Contents of SiO_2 are similar to those of the massive gabbros. Contents of Fe_2O_3* and CaO in hornblendites are similar to those of the massive gabbros (Figure 5D, C). On the other hand, only contents of Na_2O and K_2O are similar to those of the layered gabbros (Figure 5E, F). In the hornblendites, high contents of Fe_2O_3*, MgO, CaO, V, Cr, Co, and Ni, low concentrations of Sr (Tables 1, 2) are visible.

Concentrations of Nb and Ta in the hornblenditic rocks follow similar trends. There are negative Nb and Zr and moderately positive Ti anomalies in these rocks (Figure 7B). In comparison, Eu shows no anomalies (Figure 7B) in the hornblendites. The rocks exhibit REE patterns like a bell-shape. Therefore La_n/Yb_n and Sm_n/Yb_n ratios are ranges between 0.66 and 1.30 and 1.80 and 1.90. Also, the patterns (Figure 8B) are not similar to those of other rock types (Figure 8A, C).

Massive gabbros

There are higher concentrations of SiO_2, TiO_2, MgO, Fe_2O_3*, Na_2O, MnO, and K_2O and lower concentrations of CaO and Al_2O_3 in the layered gabbros compared to massive gabbros. Contents of Fe_2O_3*, Na_2O, K_2O, and SiO_2 are higher than those of the other rocks types (Table 1; Figure 5). On the other hand, X_{Mg} is lower than in the other rocks types. Similar to the layered gabbros, massive gabbros are, also, related to the tholeiitic suite (Figure 6A, B).

Compared to layered gabbros, the massive gabbros have higher concentrations of V, Cr, Rb, Sr, Ba, and REEs. There are negative Ta and Zr anomalies and slight positive or negative and/or no Nb anomalies (Figure 7C). Additionally, high concentrations of P and Ti in the massive gabbros produce positive anomalies in the spider diagram.

The rocks exhibit REE patterns as negative slope-shape from LREE to HREE. Therefore La_n/Yb_n and Sm_n/Yb_n ratios are in ranges between 1.83 and 3.23 and 1.80 and 2.11. Additionally, the patterns (Figure 8C) are not similar to those of layered gabbros (Figure 8A, C), and hence total REE in the massive gabbros are more reach than layered gabbros. There are no Eu anomalies in the rocks.

Table 2. Representative whole rock geochemical analyses (ICP-MS) of minor and rare earth elements from the Mamakan rocks.

Sample		FM-2	FM-5	FM-6	FM-9	FM-11	FM-12	FM-15	FM-22	FM-25	FM-26	FM-30	FM-31	FM-32	FM-35	FM-36
	Uncertainty	Meso	Mela	Hornb	Leuco	Leuco	Leuco	Leuco	Hornb	Hornb	Cpx-Ano	Mela	Mela	Mela	Mela	Mela
Rock type	ppm	Lay-G	Lay-G	Lay-G	Lay-G	Lay-G	Lay-G	Lay-G	Lay-G	Lay-G	Lay-G	Mas-G	Mas-G	Mas-G	Mas-G	Mas-G
Cs	0.01	0.2	0.45	0.02	<0.01	0.08	0.77	0.1	0.1	0.09	0.37	0.22	0.12	0.77	0.08	0.26
V	5	91	94	422	47	85	63	72	223	205	37	358	371	359	304	354
Cr	10	110	140	380	60	60	70	60	280	260	30	590	280	250	1140	210
Co	0.50	36.5	61.7	72.5	18.8	35.8	18.7	23.3	79.2	86.9	12.6	49.3	50.2	53.0	52.4	44.0
Ni	5	52	88	106	27	55	28	44	118	129	19	114	64	92	194	65
Rb	0.20	1.6	5.1	1.9	0.4	1.4	4.8	1.3	1.7	1.9	2.5	6.0	3.9	12.5	3.3	6.4
Sr	0.10	299	253	71	425	354	431	397	108	40	452	219	224	233	145	230
Y	0.50	3.5	3.6	14.1	1.9	2.9	2.2	2.5	8.4	8.2	1.2	20.6	29.0	21.9	16.9	22.1
Zr	2	6.0	6.0	19.0	4.0	8.0	5.0	5.0	17.0	18.0	3.0	52.0	79.0	44.0	42.0	48.0
Nb	0.20	<x	<x	1.1	<x	<x	<x	<x	0.6	0.4	<x	4.8	7.8	2.6	3.6	4.6
Ba	0.50	21.9	31.6	30.2	19.5	20.8	34.2	34.6	20.7	16.4	24.3	88.4	145.5	74.6	60.6	96.4
La	0.50	0.7	0.6	1.1	0.8	0.7	0.8	0.7	1.3	1.4	0.7	9.2	13.3	5.9	6.8	9.9
Ce	0.50	1.8	1.6	4.1	1.5	1.7	1.7	1.6	3.7	3.9	1.3	23.3	34.5	16.6	18.2	25.8
Pr	0.03	0.28	0.26	0.81	0.21	0.26	0.23	0.22	0.60	0.62	0.17	2.99	4.48	2.43	2.44	3.36
Nd	0.10	1.50	1.40	4.90	1.00	1.30	1.10	1.10	3.30	3.20	0.80	13.10	20.00	11.70	11.00	14.70
Sm	0.03	0.49	0.49	1.91	0.32	0.44	0.34	0.39	1.22	1.12	0.22	3.25	5.02	3.33	2.71	3.65
Eu	0.03	0.27	0.26	0.68	0.25	0.26	0.28	0.25	0.46	0.42	0.22	1.18	1.43	1.12	1.00	1.09
Gd	0.05	0.63	0.67	2.64	0.37	0.58	0.45	0.50	1.57	1.56	0.25	3.67	5.47	3.88	3.01	3.96
Tb	0.01	0.11	0.11	0.46	0.06	0.09	0.07	0.08	0.27	0.26	0.04	0.60	0.87	0.64	0.50	0.64
Dy	0.05	0.68	0.68	2.76	0.36	0.58	0.42	0.47	1.61	1.56	0.24	3.60	5.19	3.86	2.94	3.81
Ho	0.01	0.14	0.14	0.56	0.07	0.12	0.09	0.10	0.34	0.32	0.05	0.78	1.11	0.84	0.63	0.84
Er	0.03	0.35	0.37	1.45	0.19	0.33	0.24	0.27	0.91	0.86	0.14	2.17	3.08	2.28	1.80	2.30
Tm	0.01	0.05	0.05	0.20	0.03	0.04	0.03	0.04	0.13	0.12	0.02	0.33	0.44	0.34	0.27	0.35
Yb	0.03	0.29	0.29	1.15	0.16	0.25	0.18	0.22	0.72	0.70	0.10	2.03	2.68	2.05	1.67	2.10
Lu	0.01	0.04	0.04	0.17	0.03	0.04	0.03	0.03	0.12	0.11	0.01	0.34	0.42	0.33	0.27	0.35
Hf	0.10	0.30	0.30	0.90	0.20	0.30	0.20	0.20	0.60	0.70	<x	1.90	2.80	1.60	1.50	1.90
Ta	0.10	<x	<x	0.10	<x	<x	<x	<x	<x	<x	<x	0.30	0.40	0.10	0.20	0.30
Th	0.05	<x	<x	0.11	<x	0.05	0.06	0.06	0.17	0.30	<x	0.54	0.50	0.16	0.17	0.85
U	0.05	<x	<x	0.05	<x	<x	<x	<x	<x	0.06	<x	0.19	0.13	0.05	0.05	0.22
K		531	1486	2017	212	531	1380	425	955	743	637	6051	5733	5733	4140	6476
Ti		2128	2128	14143	1252	1877	1502	1627	5632	4631	876	11640	14268	12265	9762	10889
P		85	102	95	160	70	70	80	88	141	70	986	1479	916	1057	986
Eu*		3.28	3.38	13.25	2.04	2.98	2.31	2.61	8.17	7.80	1.39	20.47	31.12	21.28	16.95	22.59
Eu/Eu*		1.51	1.41	0.94	2.25	1.60	2.22	1.76	1.03	0.99	2.90	1.06	0.84	0.96	1.08	0.88
La_n/Yb_n		1.79	1.53	0.66	2.72	1.79	2.72	2.38	1.11	1.30	7.15	2.76	3.23	1.83	2.57	2.89
La_n/Sm_n		0.89	0.77	0.36	1.56	0.99	1.47	1.12	0.67	0.78	1.99	1.77	1.66	1.11	1.57	1.70
Gd_n/Yb_n		1.79	1.90	1.89	1.90	1.91	2.06	1.87	1.80	1.83	2.06	1.49	1.68	1.56	1.48	1.55
Sm_n/Yb_n		1.90	1.90	1.87	2.25	1.98	2.12	1.99	1.90	1.80	2.47	1.80	2.11	1.83	1.82	1.95
Th/Yb				0.10		0.20	0.33	0.27	0.24	0.43		0.27	0.19	0.08	0.10	0.40

<x = Below detection limit.

Discussion

Ultramafic rocks

In contrast with Ghaemi (2004), an ultramafic rock such as dunite and harzburgite were not found in this study within the layered gabbros, but were only found minor outcrops of wehrlite along the gabbors in the present study. Hornblendite, which alternates with layered gabbros (Figure 2E), appears to have the same primary genesis as the layered gabbro, but has overall chemistry similar to ultramafic rocks.

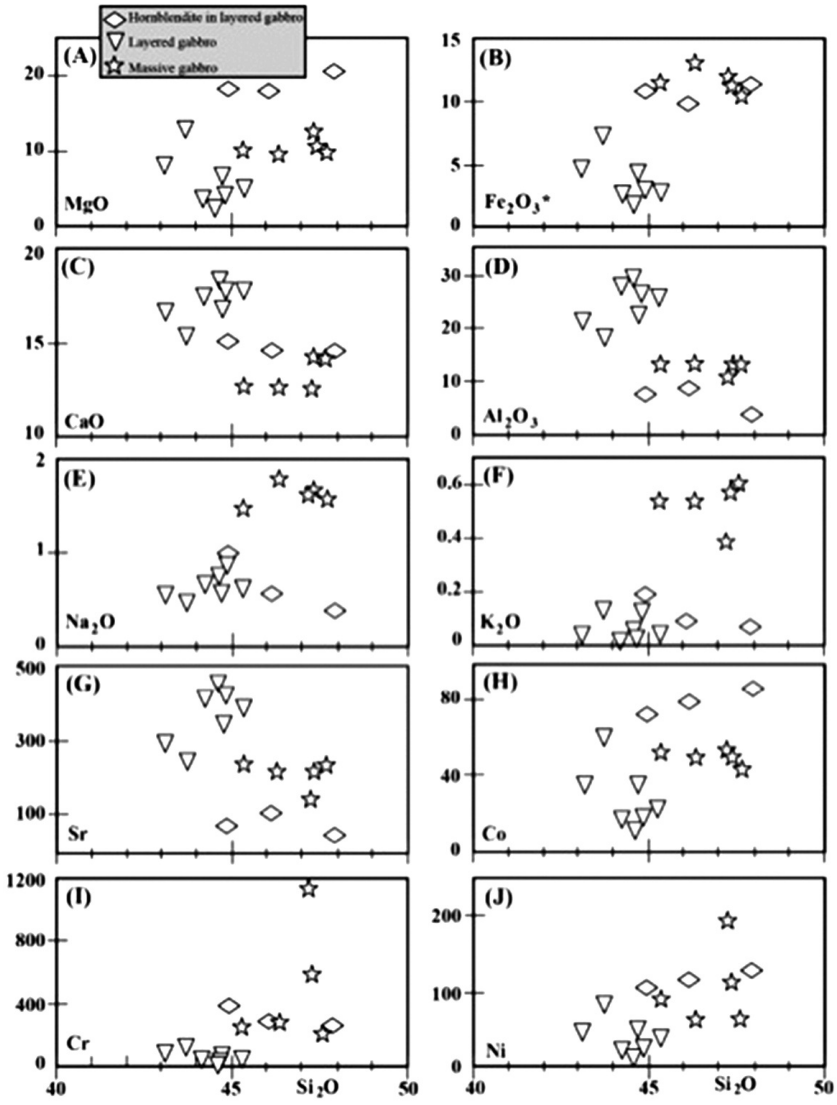

Figure 5. Binary diagrams of major element oxides vs. SiO_2.

Table 3. C.I.P.W. norm of the whole rock geochemical analyses from the Mamakan rocks.

Norm Mineral	q	or	ab	an	ne	di	hy	ol	il	hem	ap	tn	pf
Sample													
FM-2	-	0.30	4.91	56.73	-	20.64	0.20	7.95	0.17	4.91	0.02	0.20	-
FM-5	-	0.83	4.23	47.55	-	22.70	1.61	14.36	0.26	7.59	0.02	0.09	-
FM-6	-	1.12	8.04	15.26	-	43.62	-	17.86	0.34	10.90	0.02	0.75	1.10
FM-9	-	0.12	5.84	74.61	-	9.33	2.72	2.44	0.11	2.91	0.02	0.11	-
FM-11	-	0.03	4.99	60.78	-	17.90	5.71	3.33	0.15	4.58	0.02	0.17	-
FM-12	-	0.77	6.95	68.43	0.36	15.83	-	2.44	0.11	3.02	0.02	-	0.11
FM-15	-	0.24	5.42	68.23	-	15.77	4.42	1.19	0.11	3.10	0.02	0.18	-
FM-22	-	0.53	4.65	20.13	-	39.35	12.80	9.75	0.34	9.81	0.02	0.66	-
FM-25	-	0.41	3.22	8.92	-	48.75	19.20	6.84	0.43	11.35	0.05	0.36	-
FM-26	-	0.35	6.52	76.86	-	10.50	0.88	0.74	0.06	2.00	0.02	0.09	-
FM-30	-	3.37	14.13	25.75	-	32.50	8.35	1.65	0.39	11.45	0.32	1.78	-
FM-31	0.88	3.19	15.15	26.25	-	24.71	12.06	-	0.45	13.10	0.49	2.22	-
FM-32	-	3.19	12.52	27.78	-	24.88	13.06	1.00	0.41	11.60	0.30	1.88	-
FM-35	-	2.30	13.96	21.87	-	28.98	16.03	1.34	0.43	11.95	0.35	1.36	-
FM-36	1.22	3.60	13.20	26.94	-	31.57	8.90	-	0.41	10.75	0.32	1.61	-

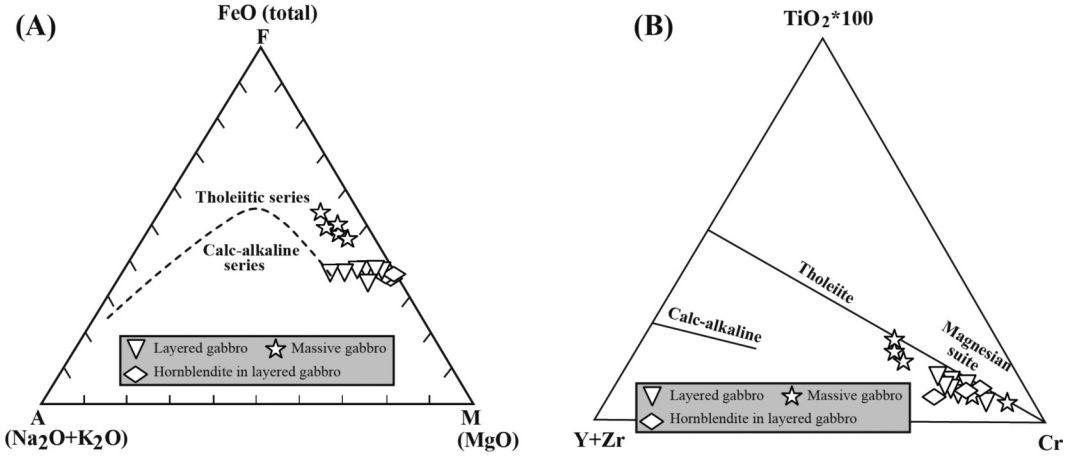

Figure 6. Chemical characteristics of the Mamakan gabbroic rocks. A) AFM (Na_2O+K_2O-FeO*+MgO wt%) discrimination diagram with field delineated after Irvine and Baragar (1971); B) Y+Zr-TiO_2*100-Cr discrimination diagram after Davies et al. (1979). All samples are plot into the tholeiite field.

Occurrence of hornblendite as lenticular shapes (Figure 2F) and of pegmatite gabbros (Figure 2G) with large minerals of hornblende and plagioclase (forming a pegmatitic appinite; see Murphy, 2013) do not support the interpretation of Chaemi (2004) of mainly metasomasim processes in the study area to form hornblendites. In addition, there is no alteration or metasomatism in the gabbros close to the hornblendites (Figure 2E). In contrast with Ghaemi (2004), therefore, hornblendites are not as a result of the metasomatism process. Gabbros and anorthosites are distinct from each other by different percentages of plagioclase and clinopyroxene, and orthopyroxene.

In some outcrops, pegmatite gabbros occur as alternating layers with hornblendites (Figure 2G). Therefore, magma chambers of the layered gabbros and related rocks (pegmatite gabbros and hornblendites) evolved in relatively ''wet'' systems (Figure 2G). These characteristic are similar to mafic parts of the appinite suites investigated by Scarrow et al. (2009) and Murphy (2013).

Magma chamber evolution

Crystallization alone yields a mafic rock, but when combined with gravitational settling (Figure 2C), new melt percolation (Figure 2B, E), convection (Figure 2F), and segregation via infiltration (Figure 2D), it leads to segregation and sorting of crystals to yield mafic to ultramafic cumulates. The cumulates, along which different new melts percolated, consist of a series of layers formed on the bottom (e.g. wehrlite and clinopyroxenite), the sides, and, through flotation (anorthosite), the top of the magma chamber. Therefore, it is possible that some layers were formed as a result of different new melt percolation within previous injections that have been crystallized (Figure 2B, E).

After the formation of the cumulates in the Mamakan layered bodies, the next pulse of magma injection caused fragmentation of the cumulates, which were at that time a crystal mush, and their dispersal throughout the magma chamber. This process caused to be occurred pieces of cumulate rocks as lenticular shapes within gabbros with cumulate texture (Figure 2D). Parts of the intrusions with gradational boundaries between gabbros and different cumulates (Figure 2C) and boundaries as suture (Figure 2E) show that either fractional crystallization or activity of two different magmas as synchronous or both was an early process during cooling of the magma chamber. It is proved by five age dating of U-Pb zircon Laser-Ablation on different layers of layered gabbros, which show ages *c.* 301 and 303 Ma (Asadpour, 2012, in press). There is no evidence of magma mixing or mingling between layered gabbros and leuco-granitic rocks. Also, the age of magma mixing (Figure 2A) between the massive gabbros and granitic rocks is slightly younger (age dating of U-Pb zircon Laser-Ablation on the massive gabbros: *c.* 300.7±1.5 Ma. and leuco-granites: *c.* 300.3±1.5 Ma; Asadpour, 2012, in press) than layered gabbros. As a result of the findings, initial magmas of layered and massive gabbros were different. In the study, no field observations were made proving the relationships between layered and massive gabbros, such as gradational transition from the layered gabbros to the massive gabbros. The contacts between layered and massive gabbros are sharp as parallel planes. Also, massive types overlie the layered gabbros.

The Mamakan intrusions are a Hercynian appinitic suite in the northwest of Iran. This suite is mainly mafic to ultramafic in composition. Although a minor felsic component (predominantly granitic or granodioritic in composition) is invariably present, there is a marked chemical bimodality. The abundance of hornblende relative to olivine and pyroxene in rocks of mafic composition and the widespread development of mafic "pegmatites" indicate that the appinitic mafic magmas were unusually

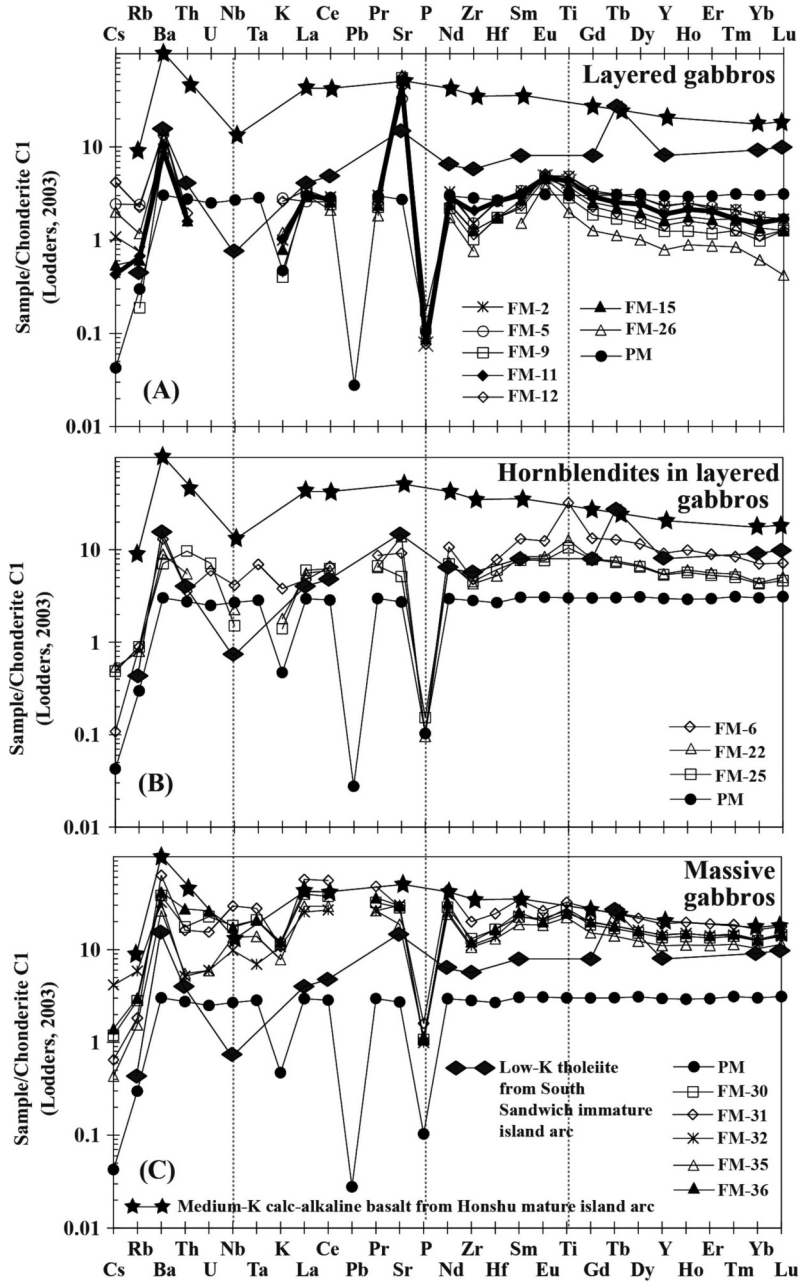

Figure 7. Primitive mantle normalized multi-element plots. A) Normalized multi-element diagram for gabbros and anorthosite in the Mamakan layered intrusions; B) Normalized multi-element diagram for hornblendites occurred in the layered intrusions. C) Normalized multi-element diagram for massive intrusions. Normalization values of the chondrite C1 after Lodders (2003). PM is primitive mantle from Sun and McDonough (1989).

enriched in H_2O (e.g., Murphy, 2013). Closed system dominated crystal fractionation controlled the evolution of the massive gabbros, whereas a combination of fractional crystallization and open system mingling took place in the inferred border rim (Figure 2A).

Appinites occur at different crustal levels, many adjacent to major steep faults that were active during their emplacement (Murphy, 2013). Such environments are consistent within contact relationships and textural observations indicating multiple phases of intrusion of compositionally bimodal magma with mixing and mingling producing rocks of intermediate composition. These faults provide conduits that would be readily exploited by fluid-rich and compositionally diverse magma.

Reaction coronas between olivine and plagioclase consists only of an orthopyroxene rim (Figure 4A, B). Moreover, hornblende crystallization from magma prior to the corona formation suggests that probably the corona formed during the post-magmatic stage. Low pressures (no more than 1 kbar pressure; Turner and Stuwe, 1992) in the presence of magma (Turner and Stuwe, 1992; Haas et al., 2002) can produce corona texture between olivine and plagioclase in unmetamorphosed gabbros. Coronas are typically produced by post-magmatic subsolidus reactions as the massifs slowly cool (e.g. Grant, 1988; Tomilenko and Kovyazin, 2008). Occurrence of altered clinopyroxene (as uralitization) and hornblende show subsolidus reactions are most probable for the study rocks.

Similar to the layered gabbros, massive gabbros are also related to the tholeiitic suite (Figure 6A, B). Also, all rock types were emplaced in an interval of 3-4 Ma. Contents of major and trace elements (Table 1), element anomalies (Figures 7 and 8), and element ratios, such as higher X_{Mg} and lower La_n/Yb_n, La_n/Sm_n, and Gd_n/Yb_n in the layered gabbros compared to those in the massive gabbros, show that there was no post-solidus transformation from layered to massive gabbros. Additionally, increases and decreases of different elements in REEs and multi-element patterns in spider diagrams, the different situation of these gabbros in Harker diagrams (Figure 5), different U-Th zircon ages of these gabbros, and plotting in different positions in the AFM diagram (Figure 6A) all demonstrate that layered and massive gabbros were not crystallized from the same initial magma. Also, based on field observations (Figure 2D, F) it is possible that fractional crystallization was not the only process during formation of the layered gabbros. Therefore, in addition to the fractional crystallization, new melt percolation (Figure 2E), convection (Figure 2F), and segregation via infiltration (Figure 2D) within chamber led to segregation and sorting of crystals to yield layering.

Petrogenesis

Variations in the concentrations of Nb and Ta in the all of the rocks follow similar trends. Ti-rich minerals such as rutile, titanite, ilmenite, amphibole, and, to a lesser extent, clinopyroxene and apatite are carriers for Nb and Ta (Xiong et al., 2005). Negative Nb and Zr and moderately positive Ti anomalies in these rocks (Figure 7B), as well as low contents of ilmenite and apatite in C.I.P.W. norms suggest that the initial magma was not enriched in these elements and that more amounts of the minerals may have been residual phases during the generation of the magma. Additionally, the behaviour of the HREEs is consistent with low concentrations of incompatible elements and with the tholeiitic composition of all samples (Figure 8A, B). Thus it is possible that spinel and rutile were major phases for sequestering Nb and Ta,, as was apatite for P, because these elements show negative anomalies in the spider diagrams (Figure 7) and also these minerals are probably stable phases during upper mantle partial melting (Xiong et al., 2005).

High concentrations of Ti in massive gabbros

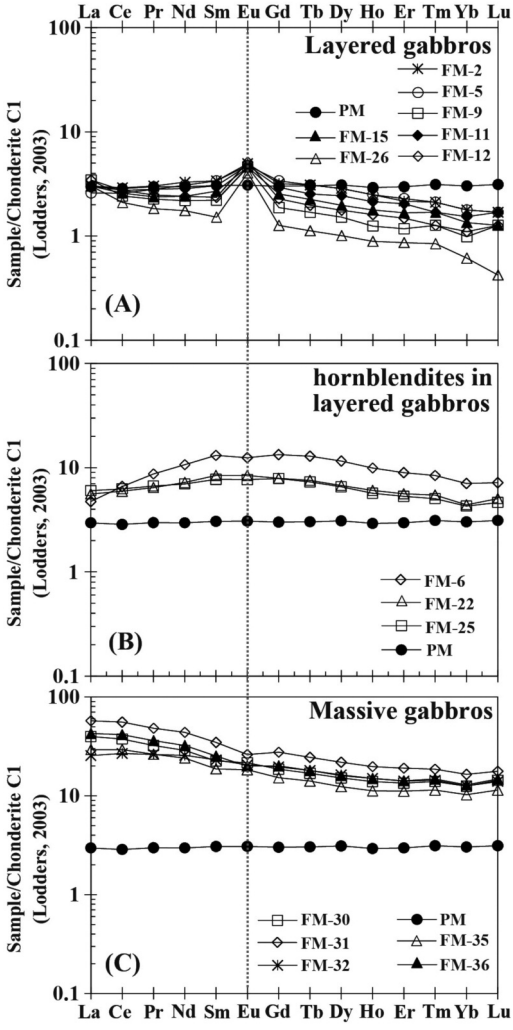

Figure 8. Primitive mantle normalized REE plots. A) Normalized REE diagram for gabbros and anorthosite in the Mamakan layered intrusions; B) Normalized REE diagram for hornblendites from the layered intrusions; C) Normalized REE diagram for massive intrusions. Normalization values of the chondrite C1 after Lodders (2003). PM is primitive mantle from Sun and McDonough (1989).

(Figure 7C; Table 1) along with higher contents of ilmenite and titanite in the C.I.P.W. norms of the massive gabbros in comparison with layered gabbros (Table 3) demonstrate that ilmenite and titanite were not probably stable minerals during partial melting of the source. It is possible that rutile and amphibole were stable solidus phases during the partial melting, because of negative Ta anomalies and slight positive or negative and/or no Nb anomalies (Figure 7C). Additionally, low ilmenite content and absence of magnetite in the C.I.P.W. norms of the study samples may result from a low partial activity of oxygen in the magma chamber.

Increasing contents of SiO_2, TiO_2, MgO, Fe_2O_3*, Na_2O, MnO, and K_2O and decreasing contents of CaO and Al_2O_3 from layered gabbros towards massive gabbros can be reflected in the decreasing modal percentages of plagioclase and the increasing modal percentages of hornblende and clinopyroxene. Massive gabbros have slight positive or negative and/or no Eu anomalies (Table 2; Figure 8A). These anomalies are supported by the occurrence of slight positive or negative and/or no Sr anomalies in these rocks (Figure 7C). The absence of a Eu anomaly suggests that the magma was oxidized, so most Eu was in the 3^+ state and did not partition into plagioclase. These observations demonstrate probably that plagioclase was not a dominant carrier for europium and strontium during the crystallization of the magma. Also it is possible that plagioclase was not a common mineral in the source during the partial melting. As in the gabbros, positive Ba anomalies in these rocks were controlled by high modal percentages of amphibole.

Some geochemical characteristics of the Mamakan gabbroic intrusions are commonly ascribed to varying mineralogies after partial melting of mafic precursors. For example, the moderate LREE/HREE enrichment (Table 2; Figure 8) and Sm/Yb vs. Sm (Figure 9A) and Sm/Yb vs. La/Sm ratios (Figure 9A) suggest

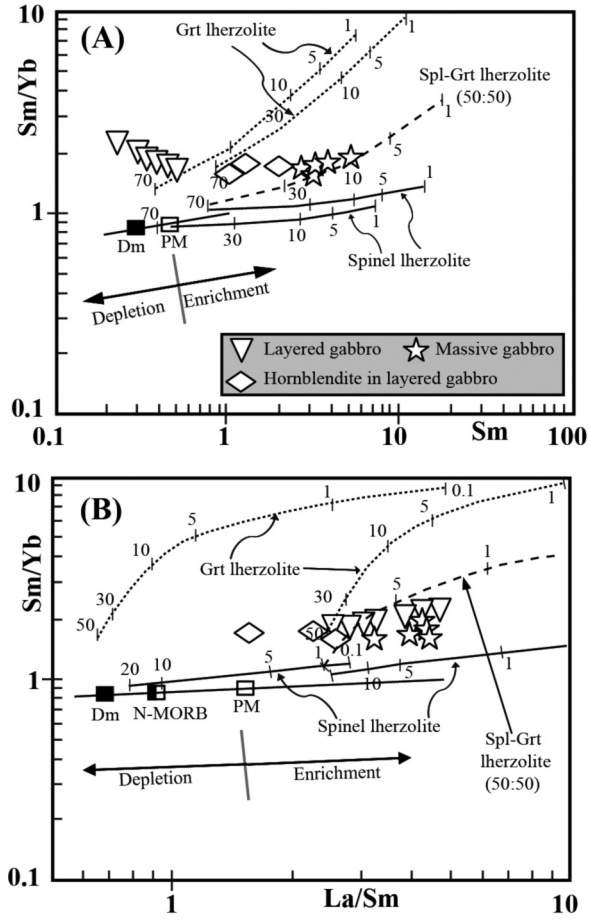

Figure 9. Plots of Sm/Yb vs. Sm (A) and Sm/Yb vs. La/Sm (B) for the gabbroic intrusions in the Mamakan gabbroic complex. Mantle array (heavy line) defined by depleted MORB mantle (DMM, McKenzie and O'Nions, 1991) and primitive mantle (PM, Sun and McDonough, 1989). Melting curves for spinel lherzolite (Ol 53 + Opx 27 + Cpx 17 + Sp 11) and garnet peridotite (Ol 60 + Opx 20 + Cpx10 + Gt 10) with both DMM and PM compositions are after Aldanmaz et al. (2000). Numbers along these lines represent the degree of the partial melting.

melting of a spinel lherzolite mantle source. Sm/Yb and La/Sm ratios and concentrations of Sm (Figures 9A, B; 10) are consistent with enriched mantle (mantle metasomatism) and suggest an contradictory role for spinel and metasomatized fluids. This is proved by positive Ba and Sr anomalies, which is probably as a result of the mantle metasomatism in the supra-subduction zone (also, see tectonic setting). Low concentrations of K are possible because K is not high in cumulate rocks, because the cumulus minerals exclude it. In addition, on a Ta/Yb vs. Th/Yb diagram (also see Zhao and Zhou, 2007 for more discussion), tholeiitic samples of the study area display a consistent trend within the main mantle metasomatism array (Figure 11A).

This suggests that there was contribution of a subduction component to the Mamakan mantle source region. The basic tholeiitic samples, especial massive gabbros, of the intrusions show a progressive shift from the MM array with increasing Na_2O and K_2O (Figure 11A). This implies that these rocks might have been derived from an enriched (spinel lherzolite) source (Figures 9 and 10) with a subduction signature (mantle metasomatism). Many of these samples display marked negative HFSE (P, Zr, Hf, Nb, and Ta) anomalies typical of magmas.

Crystallization processes

Fractional and batch melting processes and equations of them can be used to predict crystallization in the Mamakan magma chamber [see Shaw (1970) and Keskin (2005) for more discussion]. Fractional crystallization vectors (Figure 10) shows that the gabbroic rock types

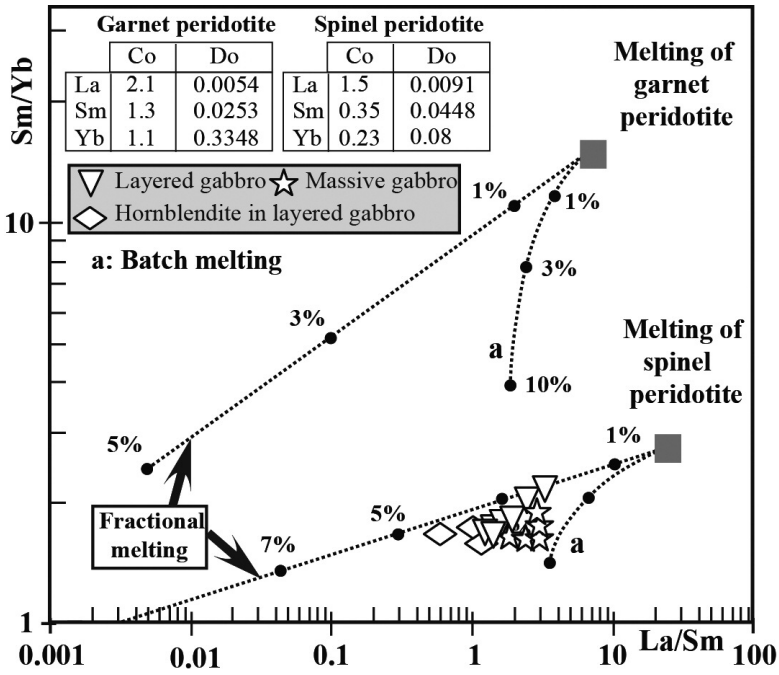

Figure 10. La/Sm vs. Sm/Yb plot showing theoretical melting curves plotted along with the basic samples from the Mamakan gabbroic intrusions. Fractional and batch melting equations of Shaw (1970) were used to construct the melting model. Numbers along these lines represent the degree of the fractional crystallization. Modal mineralogy for the spinel- and garnet-peridotites are taken from Wilson (1989), and Ol 0.66 + Opx 0.24 + Cpx 0.08 + Spl 0.02 and Ol 0.63 + Opx 0.30 + Cpx 0.02 + Grt 0.05, respectively. Trace element composition of the spinel-peridotite (Co values) is the average composition of spinel peridotite xenoliths in young (Miocene) alkaline basalts of the Thrace region, NW Turkey (after Keskin, 2005), while that of garnet peridotite is from Frey (1980). Kds between the basaltic melts and minerals given in the inset are compiled from Irving and Frey (1978), Fujimaki et al. (1984), McKenzie and O'Nions (1991) and Rollinson (1993). Bulk partition coefficient (Do) of each element has been calculated for garnet and spinel peridotite source rock compositions by taking the modal mineralogy of these end members into consideration. The coefficients are given in the inset.

and related rocks formed mostly from fractional crystallization of clinopyroxene, plagioclase, olivine, and amphibole along with accessory phases such as biotite, ilmenite and apatite.

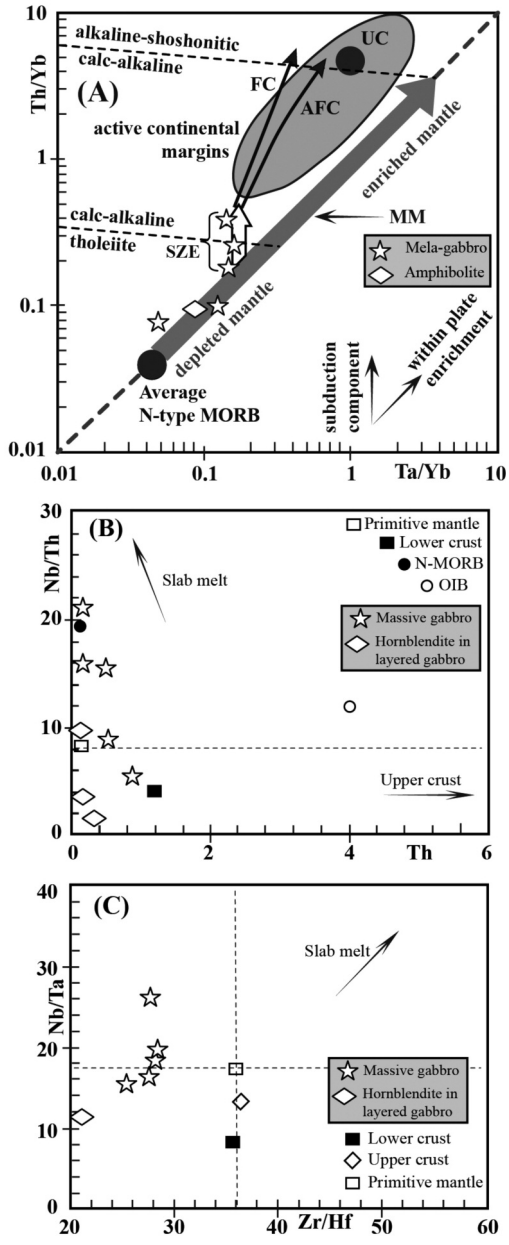

Figure 11. Plots of Th/Yb vs. Ta/Yb (A) Nb/Th vs. Th (B) and Nb/Ta vs. Zr/Hf (C) for the Mamakan gabbroic intrusions. In (A) (after Pearce, 1983), MM: mantle metasomatism array; SZE: subduction zone enrichment; UC: upper crustal composition of Taylor and McLennan (1985); FC: fractional crystallsation vector; AFC: assimilation combined with fractional crystallization curve (after Keskin, 2005). The FC curve has been modeled for 50% crystallization of an assemblage consisting of 50% plagioclase and 50% amphibole from a basic magma. The AFC vector has been drawn for an "r" value of 0.3. Note that massive-type rocks contain a distinct subduction enrichment signature. In (B) and (C) values of N-MORB, OIB and primitive mantle are from Sun and McDonough (1989). Values for the upper and lower crust are from Wedepohl (1995). Note that massive-type rocks and hornblendites from the layered gabbros contain a distinct subduction enrichment signature. Shaded area is active continental margin.

Therefore, layered and massive gabbros were separately derived from two magmatic melts extracted from the spinel lherzolite mantle source enriched by metasomatized fluids, and then advanced fractional crystallization took place during the formation of these intrusions. This is supported by similar mantle-normalized trace element patterns for each rock types (layered and massive types; Figures 7 and 8), petrographic observations, and the Th/Yb vs. Ta/Yb diagram (Figure 11A). The trends of these samples are approximately parallel to the fractional crystallization (FC) curve (Figure 10). This type of crystallization caused an increase or decrease in some incompatible elements; hence, hornblendites show bell-shape patterns, and layered and massive types are enriched in LREE (Figures 7, 8).

The abundance of the moderately incompatible elements (HREE, HFSE and Ti) is largely controlled by partial melting processes (Pearce and Peate, 1995). Thus, these elements can be used to estimate the degree of the source depletion (Woodhead et al., 1993). In particular,

HFSE are used to constrain the nature of the mantle sources, which may have been depleted by previous melt extraction in back-arc basins (Woodhead et al., 1993; Zhao and Zhou, 2007) or in arc settings (Zhao and Zhou, 2007). Experimental studies reveal that Nb-Ta and Zr-Hf have significantly different partition coefficients in the system Cpx/anhydrous (Hart and Dune, 1993; Johnson, 1998) and Nb-Ta in the system rutile/anhydrous silicate melts (Foley et al., 2000; Schmidt et al., 2004; Xiong et al., 2005). In the Cpx/melt system, Zr is generally more incompatible than Hf by a factor of 1.5-2, whereas the D_{Nb}/D_{Ta} ratio is less than 1 (Zhao and Zhou, 2007). Therefore, Nb/Ta and Zr/Hf ratios can be significantly fractionated and would be positively correlated during partial melting of the upper mantle. Arc basalts derived from a mantle wedge (slab melts) may inherit such ratios, reflecting variable degrees of mantle depletion produced prior to episodes of melt generation (Plank and White, 1995). Therefore, the correlations between Nb/Th vs. Th and Nb/Ta vs. Zr/Hf probably reveal slab melt trends (Figure 11B, C). But, very low HFSE contents and small Nb/Ta ratios in the study rocks are interpreted as reflecting melt extraction from the mantle wedge. This evidence suggests that the mantle source region of the Mamakan gabbroic intrusions was a depleted upper (lithospheric) mantle, which probably was enriched by subduction-related components.

Both the composition of the mantle source and the degree of partial melting that produced the parental magmas of these intrusions, especially the gabbros, can be determined using REE abundances and ratios. Partial melting of a spinel lherzolite mantle source does not change the Sm/Yb ratio (Figures 9A, B and 10) because both Sm and Yb have similar partition coefficients, whereas it may decrease La/Sm ratios and Sm contents of the melts (Aldanmaz et al., 2000; Keskin, 2005). Therefore, partial melts of a spinel lherzolite source should define melting trends sub-parallel to, and nearly coincident with, a mantle array defined by depleted to enriched source compositions (Green, 2006). On the other hand, garnet has a high partition coefficient for Yb (D_{garnet}/melt = 6.6) relative to Sm (D_{garnet}/melt = 0.25) (Johnson, 1994), so that partial melting of garnet-lherzolite mantle with residual garnet will produce a more steeply sloping trend on a Sm/Yb vs. Sm diagram than will melting of spinel lherzolite (Figure 9A). All rock types of the Mamakan gabbroic intrusions, especially the gabbros, have Sm/Yb ratios higher than the spinel lherzolite melting curve, but have trends approximately similar to the spinel-lherzolite melting trend (Figures 9A, B, and 10). Therefore, the melts of the intrusions may have been derived from a spinel lherzolite mantle source.

Tectonic setting

Observations of field, geochemical and isotopic age (Asadpour, in press) data on the Mamakan complex and geochemical comparisons with the low-K tholeiite from the South Sandwich immature island arc (Pearce et al., 1995; Gill, 2010) and the medium-K calc-alkaline basalt from the Honshu mature island arc (Pearce et al., 1995; Gill, 2010) show that the complex was probably related to subduction system activity at the end of the Late Carboniferous (303-298 Ma).This process is related to the subduction of the Paleotethys Ocean (Figure 12A) beneath the southern margin of supra-subduction oceanic crust jointed to the Eurasian plate (Figure 12B). Comparison of geochemical data (Figure 7A) between the Mamakan gabbroic bodies and the low-K tholeiites from South Sandwich (which are subduction-related immature island arc basalts; Pearce et al., 1995; Gill, 2010), shows that the Mamakan layered gabbros were probably formed in an immature island arc setting.

On the other hand, comparison of geochemical

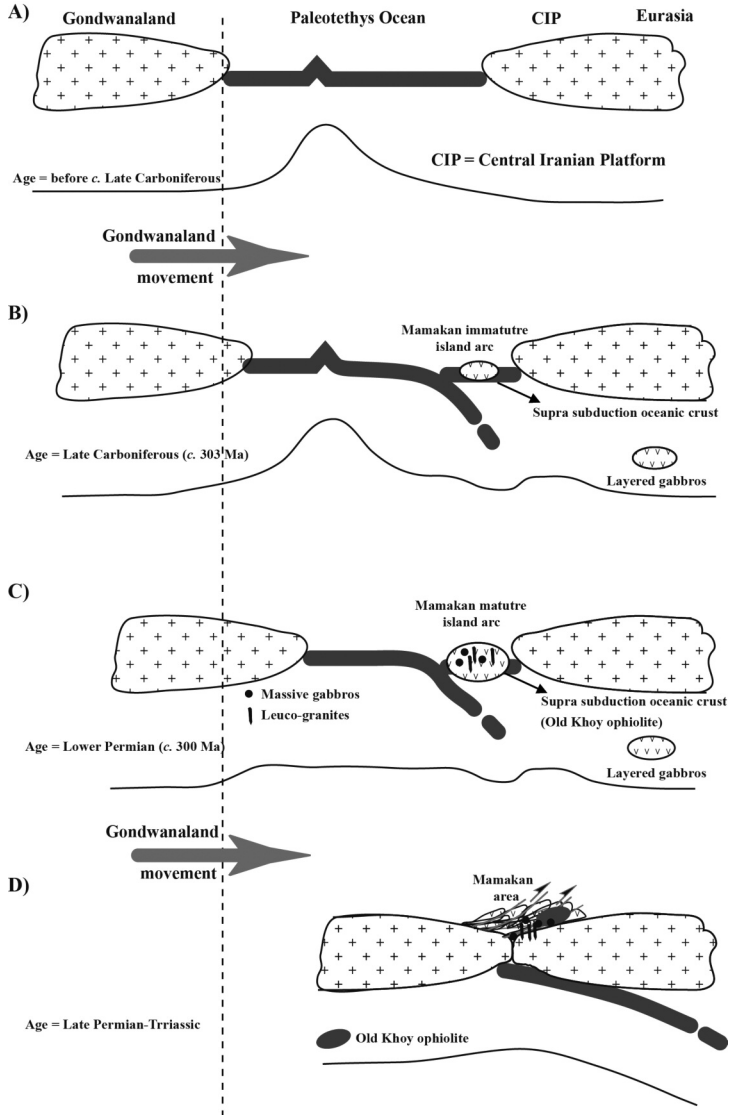

Figure 12. Tectono-magmatic evolution of the Mamakan gabbroic complex in the northwestern Iran. A) Paleotethys opening before Late Carboniferous at *c.* 303 Ma between the Gondwanaland and south central Iranian Platform (south Eurasia); B) Subduction of the Paleotethys oceanic crust beneath the supra-subduction oceanic crust demonstrates the following results: (1) formation of the immature volcanic island arc and (2) formation and injection of the layered gabbros; C) Continuation of the Paleotethys subduction beneath the supra-subduction oceanic crust at *c.* 300 Ma reveals the following results: (1) formation of the mature volcanic island arc and (2) formation and injection of the massive gabbros and leuco-granites simultaneously; D) Collision between the Gondwanaland and south central Iranian Platform (south Eurasia) and presumably emplacement of the old Khoy opholite in the Early Mesozoic. The vertical dashed line shows movement towards northeast of the Gondwanaland and closure of the Paleotethys.

data (Figure 7C) between the Mamakan gabbroic bodies and the medium-K calc-alkaline basalt from the Honshu island (Pearce et al., 1995; Gill, 2010), which are subduction-related mature island arc basalts, shows that the massive types were probably formed in more mature island arc setting in the Early Permian to Late Carboniferous (Figure 12C; based on Asadpour, 2012, in press *c.* 300.7±1.5 Ma). Magma mixing between the massive gabbros and granitic rocks (Figure 2A) demonstrate probably that there was a real continental crust at the time of emplacement of the massive gabbros (Figure 12C). This is proved by higher contents of K in the massive gabbros in relation to the layered gabbros (Table 1; Figure 7A, C). The magma that formed the massive gabbros melted crust and formed granitic liquids.

It is possible that supra-subduction oceanic crust located between the Mamakan layered-massive gabbros and continental crust to the north (probably south central Iran Block, south Eurasia) is the origin of the Khoy poly-metamorphic ophiolite (Figure 12B, C). Based on metamorphic amphiboles, the ^{40}K-^{40}Ar age of the metagabbros from the ophiolite was *c.*194.8±10.1 Ma (Khalatbari-Jafari et al., 2006). It is possible that primary magmatic age should logically be pre-Jurassic (Late Permian-Triassic?). Therefore, collision between the Mamakan island arc and Eurasia occurred presumably during the Early Mesozoic (Figure 12D) and emplaced the old Khoy ophiolite in the Early Mesozoic. In summary, subduction of the Paleotethys beneath the Mamakan island arc formed the layered and massive gabbros at 303-298 Ma (also see Mackenzie, 1972) and that old Khoy ophiolite was emplaced on the southern margin of Eurasia (central Iranian platform) in the Early Mesozoic.

Conclusions

Before the Late Carboniferous, the Paleotethys Ocean opened between Gondwanaland and Eurasia in the south central Iranian Platform around the Mamakan area. Tholeiitic melts, related to the start of Paleotethys subduction activity beneath south Mamakan island arc at *c.* 303-298 Ma, were produced from a metasomatized upper lithospheric mantle wedge at a depth consistent with the stability field of spinel lherzolite. The Mamakan layered gabbros were probably formed in an immature island arc setting in the Late Carboniferous (*c.* 301.5±1.3 Ma; Kasimovian). The Mamakan massive gabbros were a little younger and formed in more mature island arc setting in the Late Carboniferous (*c.* 300.7±1.5 Ma; Kasimovian). The tholeiitic Mamakan gabbroic intrusions have characteristics of an appinite suite. Ultramafic-mafic appinitic parts are coeval with, and emplaced into, widespread Late Carboniferous peraluminous granitoid rocks in the study area. The mafic rocks of the Mamakan intrusions display marked negative HFSE (P, Zr, Hf, Nb, and Ta) and positive Ba and K anomalies typical of subduction-related magmas. During emplacement, they underwent magmatic transformations and fractional crystallization in an open system, which was resupplied frequently, and by these processes formed cumulate gabbros, anorthosites and hornblendites in the island arc system. Mechanical forces, resulting from subsequent magma injections caused fragmentation of earlier formed anorthosite and ultramafic cumulus crystal mushes, and the scattering of the fragments throughout magma chamber. This is the cause of the heterogeneity observed in some parts of the Mamakan layered gabbroic intrusions.

Acknowledgments

The author would like to thank Mr. Mohammad Piroei for him support during field sampling. Financial support from the Iranian Ministry of Science, Research and Technology, and from the University of Urmia (Iran) are gratefully

acknowledged. The authors like to thank the Associate Editor of Periodico di Mineralogia, Dr. Georgia Pe-Piper, and the reviewers (Professor Brendan Murphy and an anonymous reviewer) of the paper for their efforts.

References

Agard P., Omrani J., Jolivert L. and Mouthereau F. (2005) - Convergence history across Zagros (Iran): constraints from collisional and earlier deformation. *International Journal of Earth Sciences (Geologische Rundschau)*, 94, 401-1.

Agard P., Omrani J., Jolivet L., Whitechurch H., Vrielynck B., Spakman,W., Monié P., Meyer B. and Wortel R. (2011) - Zagros orogeny: a subduction-dominated process. *Mineralogical Magazine*, 1-34, doi: 10.1017/S001675681100046X.

Alavi M. (1994) - Tectonic of the Zagros orogenic belt of Iran: new data and interpretations. *Tectonophysics*, 229, 211-238.

Alavi-Naini M. (1972) - Etude geologique de la region de Djam. *Geological Survey of Iran*, Report No. 23, 288 pp.

Aldanmaz E., Pearce J.A., Thirlwall M.F. and Mitchell J.G. (2000) - Petrogenetic evolution of late Cenozoic, post-collision volcanism in western Anatolia, Turkey. *Journal of Volcanology and Geothermal Research*, 102, 67-95.

Arculus R.J. and Wills K.J.A. (1980) - The petrology of plutonic blocks and inclusions from the Lesser Antilles Island Arc. *Journal of Petrology*, 21, 743-799.

Asadpour M. (2012) - Petrology and Geochemistry of Ultramafic Rocks to Medium Rocks in the Ghoushchi Region (Orumieh). PhD thesis, University of Shahid-Beheshti.

Asadpour M. (2002) - Petrology and Geochemistry of Ultramafic Rocks to Medium Rocks in the Ghoushchi Region (Orumieh). MSc thesis, University of Shahid-Beheshti.

Asadpour M. (in press) - New evidence of the Precambrian and Paleozoic magmatism in the Gharabagh massive, Northwest Iran. *Journal of Geosciences, IRI*.

Bacon C.R., Sisson T.W. and Mazdab F.K. (2007) - Young cumulate complex beneath Veniaminof caldera, Aleutian arc, dated by zircon in erupted plutonic blocks. *Geology*, 35, 491-494.

Bard J-P., Maluski H., Matte P. and Proust F. (1980) - The Kohistan sequence; crust and mantle of an obducted island arc. In: Tahirkheli R.A.K, Jan M.Q., Majid M. (eds) - Proceedings of the International Committee on Geodynamics, Group 6 meeting (*Geological Bulletin, University of Peshawar,* Peshawar, Pakistan), 87-93.

Beard J.S. and Borgia A. (1989) - Temporal variation of mineralogy and petrology in cognate gabbroic enclaves at Arenal volcano, Costa Rica. *Contributions to Mineralogy and Petrology*, 103, 110-122.

Berberian M. (1995) - Master "blind" thrust faults hidden under the Zagros folds: active basement tectonics and surface morphotectonics. *Tectonophysics*, 241, 193-5.

Berberian M. and King G.C.P. (1981) - Towards a paleogeography and tectonic evolution of Iran. *Canadian Journal of Earth Sciences*, 18, 210-265.

Bignold S., Treloar P.J. and Petford N. (2006) - Changing sources of magma generation beneath intra-oceanic island arcs: an insight from the juvenile Kohistan island arc, Pakistan Himalaya. *Chemical Geology*, 233, 46-74.

Burns L.E. (1985) - The Border Ranges ultramafic and mafic complex, south-central Alaska: cumulate fractionates of island-arc volcanics. *Canadian Journal of Earth Sciences*, 22, 1020-1038.

Conrad W.K. and Kay R.W. (1984) - Ultramafic and mafic inclusions from Adak Island: crystallization history, and implications for the nature of primary magmas and crustal evolution in the Aleutian Arc. *Journal of Petrology*, 25, 88-125.

Davidson J.P. (1996) - Deciphering mantle and crustal signatures in subduction zone magmatism. In: Bebout G.E., Scholl D., Kirby S., Platt J.P. (eds) - Subduction Top to Bottom. *American Geophysical Union, Geophysical Monograph*, 96, 251-262.

Davies J.F., Grant R. and Whitehead R.E.S. (1979) - Immobile trace elements and Archean volcanic stratigraphy in the Timmins mining area, Ontario. *Canadian Journal of Earth Sciences*, 16, 305-311.

Dercourt J., Zonenshain L.P., Ricou L.-E., Kazmin V.G., Lepichon X., Knipper A.L., Grandjacquet C., Sbortshikov I.M., Geyssant J., Lepvrier C., Pechersky D.H., Boulin J., Sibuet J.-C., Savostin L.A., Sorokhtin O., Westphal M., Bazhenov M.L., Lauer J.P. and Biju-Duval B. (1986) - Geological

evolution of the Tethys belt from the Atlantic to the Pamirs since the LIAS. *Tectonophysics*, 123, 241-315.

Dhuime B., Bosch D., Garrido C.J., Bodinier J.L., Bruguier O., Hussain S.S. and Dawood H. (2009) - Geochemical architecture of the lower- to middle-crustal section of a paleoisland Arc (Kohistan complex, Jijal-Kamila area, Northern Pakistan): implications for the evolution of an oceanic subduction zone. *Journal of Petrology*, 50, 531-569.

Foley S.F., Barth M.G. and Jenner G.A. (2000) - Rutile/melt partition coefficients for trace elements and an assessment of the influence of rutile on the trace element characteristics of subduction zone magmas. *Geochimica et Cosmochimica Acta*, 64, 933-938.

Frey F.A. (1980) - The origin of pyroxenites and garnet pyroxenites from Salt Lake Crater, Oahu, Hawaii: trace element evidence. *American Journal Sciences*, 280, 427-449.

Fujimaki H., Tatsumoto M. and Aoki K. (1984) - Partition coefficients of Hf, Zr and REE between phenocrysts and groundmasses. Proceedings of the Fourteenth Lunar and Planetary Science Conference, Part 2. *Journal of Geophysical Research*, 89, 662-672.

Ghaemi J. (2004) - Geological map of Serow (1: 100 000). Geological Survey of Iran.

Gill R. (2010) - Igneous rocks and processes: A practical guide. Wiley-Blackwell, 428 pp.

Grant S.M. (1988) - Diffusion Models for Corona Formation in Metagabbros from the Western Grenville Province, Canada. *Contributions to Mineralogy and Petrology*, 98, 49-63.

Green N.L. (2006) - Influence of slab thermal structure on basalt source regions and melting conditions: REE and HFSE constraints form the Garibaldi volcanic belt, northern Cascadia subduction system. *Lithos*, 87, 23-49.

Guarino V., Fedele L., Franciosi L., Lonis R., Lustrino M., Marrazzo M., Melluso L., Morra V., Rocco I. and Ronga F. (2011) - Mineral compositions and magmatic evolution of the calcalkaline rocks of northwestern Sardinia, Italy. *Periodico di Mineralogia*, 80, 517-545.

Haas G.J.L.M., Nijland T.G., Valbracht P.J. Maijer C., Verschure R. and Andersen T. (2002) - Magmatic versus Metamorphic Origin of Olivine-Plagioclase Coronas. *Contributions to Mineralogy and Petrology*, 143, 537-550.

Hacker B.R., Mehl L., Kelemen P.B., Rioux M., Behn M.D. and Luffi P. (2008) - Reconstruction of the Talkeetna intraoceanic arc of Alaska through thermobarometry. *Journal of Geophysical Research*, 113, B03204, doi: 10.1029/2007JB005208.

Haghipour A. and Aghanabati A. (1976) - Geological map of Serow (1:250000). Geological Survey of Iran.

Hart S.R. and Dune T. (1993) - Experimental Cpx/melt partitioning of 24 trace elements. *Contributions to Mineralogy and Petrology*, 113, 1-8.

Irvine T.N. and Baragar W.R.A. (1971) - A guide to the chemical classification of the common volcanic rocks. *Canadian Journal of Earth Sciences*, 8, 523-548.

Irving A.J. and Frey F.A. (1978) - Distribution of trace elements between garnet megacrysts and host volcanic liquidus of kimberkitic to rhyolitic composition. *Geochimica et Cosmochimica Acta*, 42, 771-787.

Johnson K.T.M. (1998) - Experimental determination of partition coefficients for rare earth and high-field-strength elements between clinopyroxene, garnet, and basaltic melt at high pressure. *Contributions to Mineralogy and Petrology*, 133, 60-68.

Johnson K.T.M. (1994) Experimental Cpx/ and garnet/melt partitioning of REE and other trace elements at high pressures; petrogenetic implications. *Mineralogical Magazine*, 58, 454-455.

Keskin M. (2005) - Domal uplift and volcanism in a collision zone without a mantle plume: Evidence from Eastern Anatolia. *www.MantlePlumes.org*.

Khadivi S., Mouthereau F., Barbarand J., Adatte T. and Lacombe O. (2012)- Constraints on paleodrainage evolution induced by uplift and exhumation on the southern flank of the Zagros-Iranian Plateau. *Journal of Geological Society of London*, 169, 83-97.

Khalatbari-Jafaria M., Juteau T. and Cotton J. (2006) - Petrological and geochemical study of the Late Cretaceous ophiolite of Khoy (NW Iran), and related geological formations, Iran. *Journal of Asian Earth Sciences*, 27, 465-502.

Lodders K. (2003) - Solar system abundances and condensation temperatures of the elements. *Astrophysical Journal*, 591, 1220-1247.

Mackenzie D.P. (1972) - Active tectonics of the Mediterranean Region. *Geophysical Journal International*, 30, 109-185.

McKenzie D.P. and O'Nions R.K. (1991) - Partial melt

distribution from inversion of rare earth element concentrations. *Journal of Petrology*, 32, 1021-1091.

Mohajjel M., Fergusson C.L. and Sahandi M.R. (2003) - Cretaceous-Tertiary convergence and continental collision, Sanandaj-Sirjan zone, Western Iran. *Journal of Asian Earth Sciences*, 21, 397-412.

Mouthereau F., Lacombe O. and Vergés J. (2012) - Building the Zagros collisional orogen: Timing, strain distribution and the dynamics of Arabia/Eurasia plate convergence. *Tectonophysics*, 532-535, 27-60.

Nabavi M.H. (1976) - Principle of Iran Geology. Geological Survey of Iran, 109 pp.

Nicotra E., Ferlito C., Viccaro M. and Cristofolini R. (2011) - Volcanic geology and petrology of the Val Calanna succession (Mt. Etna, Southern Italy): discovery of a new eruptive center. *Periodico di Mineralogia*, 80, 287-307.

Omrani J., Agard P., Whitechurch H., Benoit M., Prouteau G. and Jolivet L. (2008) - Arc magmatism and subduction history beneath the Zagros Mountains, Iran: a new report of adakites and geodynamic consequences. *Lithos*, 106, 380-398.

Pallato P., Mulch A., Landgraf A., Strecker M.R., Dalconi M.C., Friedrich A. and Tabatabaei S.H. (2010) - Middle to late Miocene Middle Eastern climate from stable oxygen and carbon isotope data, southern Alborz mountains, N Iran. *Earth and Planetary Science Letters*, 300, 125-38.

Paul A., Hatzfeid D., Kaviani A., Tatar M. and Pequegnat C. (2010) - Seismic imaging of the lithospheric structure of the Zagros mountain belt (Iran). In: Leturmy P., Robin C. (eds) - Tectonic and Stratigraphic Evolution of Zagros and Makran during the Mesozoic-Cenozoic. *Geological Society of London, Special Publication*, 330, 5-18.

Pearce J.A. (1983) - The role of sub-continental lithosphere in magma genesis at destructive plate margins. In: Hawkesworth C.J., Norry M.J. (eds) - In continental basalts and mantle xenoliths. *Nantwich, Shiva*, 230-249.

Pearce J.A., Baker P.E., Harvey P.K. and Luff I.W. (1995) - Geochemical evidence for subduction fluxes, mantle melting and fractional crystallization beneath the South Sandwich-Island Arc. *Journal of Petrology*, 36, 1073-1109.

Pearce J.W. and Peate D.W. (1995) - Tectonic implications of the composition of volcanic arc magmas. *Annual Review of Earth and Planetary Sciences*, 23, 251-285.

Peate D.W., Pearce J.A., Hawkesworth C.J., Colley H., Edwards C.M.H. and Hirose K. (1997) - Geochemical variations in Vanuatu arc lavas: the role of subducted material and a variable mantle wedge composition. *Journal of Petrology*, 38, 1331-1358.

Petterson M.G. (2010) - A review of the geology and tectonics of the Kohistan island arc, north Pakistan. In: Kusky T.M., Zhai M.G., Xiao W. (eds) - The Evolving Continents: Understanding Processes of Continental Growth. *Geological Society of London, Special Publications*, 338, 287-327.

Plafker G., Nokleberg W.J. and Lull J.S. (1989) - Bedrock geology and tectonic evolution of the Wrangellia, Peninsular, and Chugach terranes along the Trans-Alaskan Crustal Transect in the northern Chugach Mountains and southern Copper River basin, Alaska. *Journal Geophysical Research*, 94, 4255-4295.

Plank T. and White W.M. (1995) - Nb and Ta in arc and mid-ocean basalts. *AGU Fall Meeting Abstracts, EOS*, 76 (Suppl.), 655.

Rioux M., Mattinson J., Hacker B., Kelemen P., Blusztajn J., Hanghøj K. and Gehrels G. (2010) - Intermediate to felsic middle crust in the accreted Talkeetna arc, the Alaska Peninsula and Kodiak Island, Alaska: an analogue for low-velocity middle crust in modern arcs. *Tectonics*, 29, doi: 10.1029/2009TC002541.

Rollinson H.R. (1993) - Using geochemical data: evaluation, presentation, interpretation. Longman Scientific and Technical, John Wiley Sons, New York, 352 pp.

Romengo N., Patrizia Landi P. and Rotolo S.G. (2012) - Evidence of basaltic magma intrusions in a trachytic magma chamber at Pantelleria (Italy). *Periodico di Mineralogia*, 81, 163-178.

Scarrow J.H., Molina J.F., Bea F. and Montero P. (2009) Within-plate calc-alkaline rocks: Insights from alkaline mafic magma-peraluminous crustal melt hybrid appinites of the Central Iberian Variscan continental collision. *Lithos*, 110, 50-54.

Schaltegger U., Zeilinger G., Frank M. and Burg J-P. (2002) - Multiple mantle sources during island arc magmatism: U-Pb and Hf isotopic evidence from the Kohistan arc complex, Pakistan. *Terra Nova*, 14, 461-468.

Schmidt M.W., Dardon A., Chazot G. and Vannucci R. (2004) - The dependence of Nb and Ta rutile-melt

partitioning on melt composition and Nb/Ta fractionation during subduction processes. *Earth and Planetary Science Letters*, 226, 415-432.

Shaw D.M. (1970) - Trace element fractionation during anatexis. *Geochimica et Cosmochimica Acta*, 34, 237-243.

Sigmarsson O., Martin H. and Knowles J. (1998) - Melting of subducting oceanic crust from U-Th disequilibria in austral Andean lavas. *Nature*, 394, 566-569.

Stampfli G.M. and Borel G.D. (2002) - A plate tectonic model for the Paleozoic and Mesozoic constrained by dynamic plate boundaries and restored synthetic oceanic isochrons. *Earth and Planetary Science Letters*, 196, 17-33

Stöcklin J. (1968) - Structural history and tectonics of Iran: a review. *American Association of Petroleum Geologists,* 52, 1229-1258.

Sun S.S. and McDonough W.F. (1989) - Chemical and isotopic systematic of oceanic basalts: implications for mantle composition and processes. In: Saunders A.S., Norry M.J. (eds) - Magmatism in Ocean. *Geological Society of London, Special Publication*, 313-345.

Suyehiro K., Takahashi N., Ariie Y., Yokoi Y., Hino R., Kanazawa T., Hirata N., Tokuyan H. and Taira A. (1996) - Continental crust, crustal underplating and low-Q upper mantle beneath an oceanic island arc. *Science*, 272, 390-392.

Taylor S.R. and McLennan S.M. (1985) - The continental crust: its composition and evolution. Blackwell Scientific Publications, London, 312 pp.

Tomilenko A.A. and Kovyazin S.V. (2008) - Development of Corona Textures around Olivine in Anorthosites of the Korosten' Pluton, Ukrainian Shield: Mineralogy, Geochemistry, and Fluid Inclusions. *Petrology*, 16, 87-103.

Treloar P.J., Petterson M.G., Jan M.Q. and Sullivan M.A. (1996) - A reevaluation of the stratigraphy and evolution of the Kohistan arc sequence, Pakistan Himalaya: implications for magmatic and tectonic arc building processes. *Journal of Geological Society, London*, 153, 681-693.

Turner S. and Stuwe K. (1992) - Low-pressure corona textures between olivine and plagioclase in unmetamorphosed gabbros from Black Hill, South Australia. *Mineralogical Magazine*, 56, 503-509.

Wedepohl K.H. (1995) - The composition of the continental crust. *Geochimica et Cosmochimica Acta*, 59, 1217-1232.

Wilson M. (1989) - Igneous petrogenesis: a global tectonic approach. Springer, Netherlands, 466 pp.

Woodhead J.D., Eggins S. and Gamble J. (1993) - High field strength and transition element systematics in island arc and back-arc basin basalts: evidence for a multiphase melts extraction and a depleted mantle wedge. *Earth Planetary Science Letters*, 144, 491-504.

Xiong X.L., Adam T.J. and Green T.H. (2005) - Rutile stability and rutile/melt HFSE partitioning during partial melting of hydrous basalt: implications for TTG genesis. *Chemical Geology*, 218, 339-359.

Zhao J-H. and Zhou M-F. (2007) - Geochemistry of Neoproterozoic mafic intrusions in the Panzhihua district (Sichuan Province, SW China): Implications for subduction-related metasomatism in the upper mantle. *Precambrian Research*, 152, 27-47.

Submitted, February 2013- Accepted, May 2013